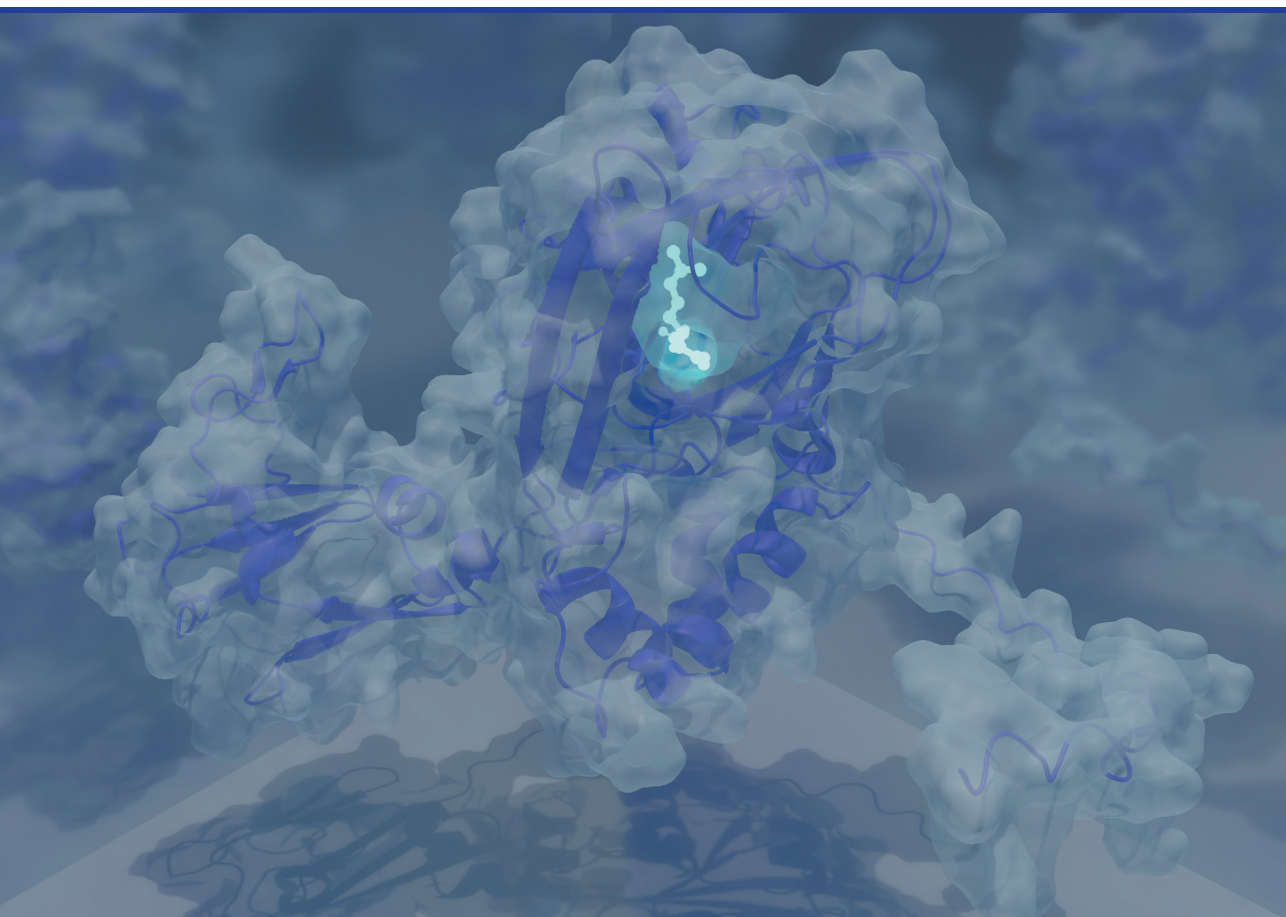


Diāna Zeļencova-Gopejenko

**STRUCTURAL AND FUNCTIONAL STUDIES OF
PROTEINS INVOLVED IN THE REGULATION OF
FATTY ACID METABOLISM**

Summary of the Doctoral Thesis



RIGA TECHNICAL UNIVERSITY
Faculty of Materials Science and Applied Chemistry
Institute of Applied Chemistry

Diāna Zelencova-Gopejko
Doctoral Student of the Study Programme “Chemistry”

**STRUCTURAL AND FUNCTIONAL STUDIES
OF PROTEINS INVOLVED
IN THE REGULATION OF FATTY ACID
METABOLISM**

Summary of the Doctoral Thesis

Scientific Supervisor
Dr. chem. KRISTAPS JAUDZEMS

RTU Press
Riga 2023

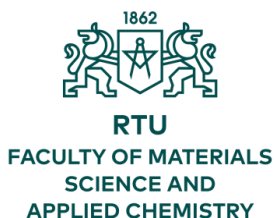
Zelencova-Gopejenko, D. Structural and Functional
Studies of Proteins Involved in the Regulation
of Fatty Acid Metabolism.
Summary of the Doctoral Thesis.
Riga: RTU Press, 2023. – 52 p.

Published in accordance with the decision of
Promotion Council “RTU P-01” of 23 March 2023,
No. 04030-9.1/41.

This research was conducted in the Department of Physical Organic Chemistry of Latvian Institute of Organic Synthesis from 2015 to 2023.

The research received funding from the Latvian Institute of Organic Synthesis student grants IG-2020-02, IG-2021-02, IG-2022-04, and IG-2023-04.

Cover picture by Diāna Zeļencova-Gopejenko



<https://doi.org/10.7250/9789934229114>
ISBN 978-9934-22-911-4 (pdf)

DOCTORAL THESIS PROPOSED TO RIGA TECHNICAL UNIVERSITY FOR THE PROMOTION TO THE SCIENTIFIC DEGREE OF DOCTOR OF SCIENCE

To be granted the scientific degree of Doctor of Science (Ph. D.), the present Doctoral Thesis has been submitted for the defence at the open meeting of RTU Promotion Council on 21 June 2023 at 14:00 at the Faculty of Materials Science and Applied Chemistry of Riga Technical University, 3 Paula Valdena Street, Room 272.

OFFICIAL REVIEWERS

Researcher Ph. D. Gints Kalniņš
Latvian Biomedical Research and Study Centre, Latvia

Professor Dr. habil. biol. Ruta Muceniece
University of Latvia, Latvia

Lead Researcher Dr. chem. Dace Rasiņa
Latvian Institute of Organic Synthesis, Latvia

DECLARATION OF ACADEMIC INTEGRITY

I hereby declare that the Doctoral Thesis submitted for the review to Riga Technical University for the promotion to the scientific degree of Doctor of Science (Ph. D.) is my own. I confirm that this Doctoral Thesis had not been submitted to any other university for the promotion to a scientific degree.

Diana Zelencova-Gopejenko (signature)

Date:

The Doctoral Thesis has been written in Latvian. It consists of an Introduction, 3 chapters, Conclusions, 142 figures, 20 tables, 24 appendices; the total number of pages including appendices is 221. The bibliography contains 295 titles.

ANNOTATION

The Doctoral Thesis is devoted to structure-activity relationship studies of γ -butyrobetaine dioxygenase (BBOX), ϵ -trimethyl-*L*-lysine dioxygenase (TMLD), and heart-type fatty acid binding protein (FABP3) ligands. Protein-ligand binding was determined and characterized by means of isothermal titration calorimetry (ITC), nuclear magnetic resonance (NMR), and molecular modelling. A protocol for molecular dynamics of metalloproteins was developed and successfully applied for simulations of BBOX and TMLD mimetics. Key structural elements for substrate binding to BBOX and TMLD mimetics were determined in combination with substrate association/dissociation studies. Two new ITC approaches were established and implemented for the determination of ligand binding thermodynamics to TMLD and FABP3. The pharmacophore model for potential TMLD inhibitors was designed based on the experimental data. A new class of FABP3 substrates with a different binding mechanism in comparison to fatty acids was found.

Keywords: BBOX, TMLD, FABP3, NMR, ITC, MOLECULAR DOCKING, MOLECULAR DYNAMICS

CONTENTS

ABBREVIATIONS.....	7
GENERAL OVERVIEW OF THE THESIS	9
Introduction	9
The Aims of the Doctoral Thesis	10
The Objectives Defined for the Implementation of the Doctoral Thesis	10
Scientific Novelty and Main Results.....	10
Practical Application	10
Structure and Length of the Thesis	11
Approbation of the Research Results, Publications, and Thesis	11
1. SUMMARY OF LITERATURE REVIEW	13
1.1. BBOX and TMLD enzymes	13
1.2. FABP3 transport protein	15
2. SUMMARY OF RESULTS AND DISCUSSION.....	16
2.1. Design of the TMLD mimetics based on BBOX.....	16
2.1.1. Protocol development for the MD simulations of <i>in silico</i> BBOX mutants..	16
2.1.2. MD simulations of the BBOX mutants.....	16
2.1.3. Production of <i>in vitro</i> BBOX-4m and 2m mutants. Enzymatic tests.....	17
2.1.3.1. Production of BBOX-4m	17
2.1.3.2. Production of BBOX-2m	17
2.1.3.3. Enzymatic tests of MBP-BBOX-4m and MBP-BBOX-2m.....	17
2.2. Design of the TMLD model by artificial intelligence (AlphaFold).....	19
2.3. Optimization of large-scale production of active MBP-TMLD	20
2.3.1. Optimization of expression and purification conditions.....	20
2.3.1.1. Tests of the expression media	20
2.3.1.2. Search for stabilizing conditions using the TSA method	21
2.3.1.3. Tests of stabilizing additives during the sonication of the cells.....	21
2.3.2. The effect of EDTA on MBP-TMLD	23
2.4. Development of the ITC assay for MBP-TMLD enzyme	23
2.5. Study of structure-activity relationship of TMLD	24
2.5.1. Studies of binding relationships of TML analogues	24
2.5.2. Development of the pharmacophore model	29
2.5.3. Study of the enzymatic reaction of TMLD	31
2.6. Lipoprotective properties of FABP3 at the cellular level. Establishing a hypothesis	31
2.7. Experimental conditions search for FABP3 thermodynamic studies	32
2.7.1. Exploration of additives for solubility and stabilization of FAs solutions	32
2.7.2. Effect of additives on FABP3 structure	33
2.7.3. Effect of the stabilizing additives on binding thermodynamics parameters ..	34
2.7.4. Determination of binding heat capacity of FABP3-laurate	35
2.8. Thermodynamic studies of FABP3.....	36
2.8.1. Binding thermodynamics of FABP3-FA	36

2.8.2. Binding thermodynamics of FABP3-acylcarnitines and palmitoyl-CoA	37
2.8.3. Studies of saturated FA carnitine esters.....	37
2.9. Effect of palmitoyl carnitine on FABP3 at low pH	38
2.10. Validation of binding to FABP3 by NMR.....	39
2.10.1. Basic principles of chemical shift perturbation analysis.....	39
2.10.2. CSP Analysis of FABP3-ligand complexes.....	40
2.10.3. Modelling of FABP3-acylcarnitine complexes by IFD calculations	41
2.11. Studies on binding mechanism of monounsaturated acylcarnitines	42
2.12. Expanding the substrate scope of FABP3.....	45
MAIN RESULTS OF THE THESIS	46
CONCLUSIONS	47
REFERENCES.....	48
ACKNOWLEDGEMENTS	52

ABBREVIATIONS

1D	one dimensional
2D	two dimensional
3D	three dimensional
α KG	α -ketoglutarate
BBOX	γ -butyrobetaine dioxygenase
BSA	bovine serum albumin
CMC	critical micelle concentration
CoA	coenzyme A
CSP	chemical shift perturbation
DLS	dynamic light scattering
DMPC	dimyristoylphosphatidylcholine
DSBH	double-stranded β -helix motif
<i>E. Coli</i>	<i>Escherichia Coli</i>
EDTA	ethylenediaminetetraacetic acid
FA	fatty acid
FABP3	fatty acid binding protein 3
GBB	γ -butyrobetaine
GroEL/ES	molecular chaperones
HEPES	2-[4-(2-hydroxyethyl)piperazin-1-yl]ethane-1-sulphonic acid
HTML	β -hydroxy- ϵ -trimethyl-L-lysine
IC ₅₀	half-maximal inhibitory concentration
I/R	ischaemia/reperfusion
IFD	induced fit docking
ITC	isothermal titration calorimetry
ppm	parts per million
kDa	kilodaltons
NMR	nuclear magnetic resonance
KPi	potassium phosphate buffer
LC ₅₀	half-maximal lethal concentration
MBP	maltose binding protein
MD	molecular dynamics
mRNA	messenger ribonucleic acid
OGA	<i>N</i> -oxalyglycine
PDB	protein data bank
PIPES	2,2'-(piperazine-1,4-diyl)di(ethane-1-sulfonic acid)
RMSD	root mean square deviation
RMSF	root mean square fluctuation
S/H	ratio of succinate formation to hydroxylation
SASA	solvent accessible surface area
SDS-PAGE	sodium dodecyl sulphate-polyacrylamide gel electrophoresis

SEC	size exclusion chromatography
TML	ϵ -trimethyl- <i>L</i> -lysine
TMLD	ϵ -trimethyl- <i>L</i> -lysine dioxygenase
<i>TMLHE</i>	gene coding ϵ -trimethyl- <i>L</i> -lysine dioxygenase
TSA	thermal shift assay
Tris	2-amino-2-(hydroxymethyl)-1,3-propanediol

GENERAL OVERVIEW OF THE THESIS

Introduction

Cardiovascular diseases are the most common cause of death worldwide. In total, they accounted for 31.4 % of deaths in 2016, 52.8 % of which were caused by ischemic heart disease [1]. Myocardial ischemia is characterized by insufficient oxygen supply to the heart muscle, which in most cases is caused by atherosclerosis. The proportion of ischemic heart disease among all causes of death is increasing due to the ageing of the world population. As a result, there is an acute demand for new highly effective cardioprotective drugs that would significantly increase life expectancy and improve its quality. On the other hand, the successful development of medicine requires a detailed study of cardiac metabolic pathways.

To ensure contraction functions and blood circulation, heart metabolism acts as an “omnivorous” and obtains energy (in the form of adenosine triphosphate) from various energy sources, mainly using fatty acids (FA) and glucose. Normal cardiac metabolism is disrupted during ischemia/reperfusion (I/R) condition resulting in changes in the availability of the substrates and accumulation of the reactive oxygen species, toxic lipid oxidation intermediates, FA-coenzyme A (CoA) and carnitine esters [2]. Long-chain acyl-CoAs are bound to the acyl-CoA-binding protein with high affinity, thus protecting cells from their high reactivity and toxicity. However, the protective mechanisms against undesirable effects of long-chain acylcarnitines in the cells have not been studied yet. It is proposed that fatty acid-binding protein 3 (FABP3) which transports FAs from the cell membrane into the mitochondria is able to bind not only FAs but also their carnitine esters [3, 4].

Myocardial damage caused by I/R can be significantly reduced by lowering the concentration of long-chain FAs and acylcarnitines in the cell. This is a novel approach in the development of cardioprotective medicines based on the inhibition of the formation of acylcarnitines in mitochondria. One of the effective regulatory methods would be the reduction of the availability of *L*-carnitine by affecting its biosynthesis and transport. Meldonium (invented in Latvia) is an inhibitor of the γ -butyrobetaine dioxygenase (BBOX) that implements this approach. However, high doses of meldonium are required to achieve a therapeutic effect. As a result, ϵ -trimethyl-*L*-lysine dioxygenase (TMLD) is proposed as a new therapeutic target for the development of potential cardioprotective medicines. TMLD is the first enzyme in *L*-carnitine biosynthesis that catalyses the stereospecific hydroxylation of ϵ -trimethyl-*L*-lysine (TML) to hydroxy-TML similarly to BBOX (the fourth enzyme). Recent studies revealed [5] that inactivation of the *TMLHE* gene in *knock-out* mice lowered levels of long-chain acylcarnitines and decreased oxidation of FAs. Thus, a significant reduction in the infarct size (by volume of the affected cells) was also observed. These findings promote TMLD as a new therapeutic target for the design of cardioprotective medicines. However, the rational design of inhibitors is complicated due to the absence of the experimental 3D structure of TMLD (so far, all crystallization attempts have been unsuccessful).

The Aims of the Doctoral Thesis

1. Find the pharmacophores important for the ligand binding and model the structure of the active site of TMLD to develop the design of *de novo* inhibitors.
2. Explore the ability of FABP3 to bind long-chain acylcarnitines and elucidate the binding mechanism that is responsible for the protection of the cells from acylcarnitine-induced damage.

The Objectives Defined for the Implementation of the Doctoral Thesis

1. Prepare mimetics of TMLD based on the BBOX structure and evaluate binding of the native substrate and its analogues *in silico* and *in vitro*.
2. Explore binding thermodynamics and conversion rates in enzymatic reaction with TMLD of the native substrate and its analogues.
3. Determine binding affinities and thermodynamics of FABP3 binding with FA of variable length and corresponding carnitine esters.
4. Explore the binding mechanism of acylcarnitines to FABP3.

Scientific Novelty and Main Results

Within the framework of the Doctoral Thesis, the regulation possibilities of *L*-carnitine biosynthesis and FA metabolism for the design of new medicines were examined.

1. Binding thermodynamics and conversion rates in the enzymatic reaction of the potential TMLD inhibitors were investigated.
2. Important pharmacophores for the ligand binding and structural key elements contributing to the inhibition of TMLD were determined.
3. The lipoprotective effect and the ability of FABP3 to protect cells from the toxicity of acylcarnitines was confirmed.
4. A novel approach for the evaluation of the binding of long-chain FAs with FABP3 in water buffers by means of isothermal titration calorimetry (ITC) was developed.
5. The mechanism of acylcarnitines binding to FABP3 was determined.

Practical Application

Versatile and comprehensive studies of protein-ligand interactions and elucidation of the binding mechanism are important in the determination of the structure-activity relationship that can be used for *de novo* inhibitor design. Additional knowledge about protein dynamics can facilitate hit-to-lead structure optimization of the new medicines.

Structure and Length of the Thesis

The Doctoral Thesis is dedicated to structural and functional studies of the proteins BBOX, TMLD, and FABP3 that are involved in the regulation of FAs metabolism. The Thesis is written in Latvian with a total of 221 pages including appendices.

Approbation of the Research Results, Publications, and Thesis

The Doctoral Thesis includes the following publications in peer-reviewed international journals

1. **Zelencova-Gopejenko, D.**; Videja, M.; Grandane, A.; Pudnika-Okinčica, L.; Sipola, A.; Vilks, K.; Dambrova, M.; Jaudzems, K.; Liepinsh, E. Heart-Type Fatty Acid Binding Protein Binds Long-Chain Acylcarnitines and Protects Against Lipotoxicity. *Int. J. Mol. Sci.* **2023**, *24* (6), 5528.
2. **Zelencova-Gopejenko, D.**; Grandane, A.; Loza, E.; Lola, D.; Sipola, A.; Liepinsh, E.; Arsenyan, P.; Jaudzems, K. Binding versus Enzymatic Processing of ϵ -Trimethyllysine Dioxygenase Substrate Analogues. *ACS Med. Chem. Lett.* **2022**, *13* (11), 1723–1729.
3. Tars, K.; Leitans, J.; Kazaks, A.; **Zelencova, D.**; Liepinsh, E.; Kuka, J.; Makrecka, M.; Lola, D.; Andrianovs, V.; Gustina, D.; Grinberga, S.; Liepinsh, E.; Kalvinsh, I.; Dambrova, M.; Loza, E.; Pugovics, O. Targeting Carnitine Biosynthesis: Discovery of New Inhibitors against γ -Butyrobetaine Hydroxylase. *J. Med. Chem.* **2014**, *57* (6), 2213–2236.

The results of the Doctoral Thesis were presented at the following conferences

1. **Zelencova-Gopejenko D.**; Jaudzems K. Binding Specificity and Thermodynamics of Fatty Acids and Acylcarnitines Affinity to Heart-Type Fatty Acid Binding Protein. *2nd Drug Discovery Conference*. September 22–24, **2022**, Riga, Latvia.
2. **Zelencova-Gopejenko D.**; Metlans R.; Jaudzems K. Insights into binding specificity of human heart-type fatty-acid binding protein. *7th International Electronic Conference on Medicinal Chemistry*. November 1–30, **2021**, sciforum-053367 (<https://sciforum.net/event/ECMC2021>).
3. **Zelencova D.**; Vilks K.; Makrecka-Kuka M.; Liepinsh E.; Jaudzems K. Investigation of protective effects of fatty acid binding protein 3 against long-chain fatty acid derivative-induced damage. *6th International Electronic Conference on Medicinal Chemistry*. November 1–30, **2020**, sciforum-040478 (<https://ecmc2020.sciforum.net>).
4. **Zelencova D.**; Liepinsh E. Mapping the Active Site of epsilon-Trimethyllysine Hydroxylase. *Biochem. Mol. Biol. J.*, **2018**, *04*, 47. *10th Edition of International Conference on Structural Biology*, Barcelona, Spain.
5. **Zelencova D.**; Liepiņš E. Mapping of the Active Site of ϵ -Trimethyllysine Hydroxylase. *Paul Walden 10th Symposium on Organic Chemistry*, Riga, Latvia. **2017**.
6. **Zelencova D.**; Liepinsh E. Inhibitor Studies of Epsilon-Trimethyllysine Hydroxylase by Means of NMR and Computer Modelling. *EUROMAR-2016*, Aarhus, Denmark, **2016**, 433.
7. **Zelencova, D.**; Liepinsh E. Structural Models and Binding Studies of Epsilon-Trimethyllysine Hydroxylase. *MSAC 2016*, 196–200.

8. **Zelencova D.**; Liepinsh E. ϵ -Trimethyllysine Hydroxylase. Search of Inhibitors. *Drug Discovery Conference*, Riga, Latvia, **2015**, 166.

Other publications by the author

1. **Zelencova-Gopejenko, D.**; Andrianov, V.; Domracheva, I.; Kanepe-Lapsa, I.; Milczarek, M.; Stojak, M.; Przyborowski, K.; Fedak, FA.; Walczak, M.; Kramkowski, K.; Wietrzyk, J.; Chłopicki, S.; Kalvins, I. Aromatic Sulphonamides of Aziridine-2-Carboxylic Acid Derivatives as Novel PDIA1 and PDIA3 Inhibitors. *J. Enzyme Inhib. Med. Chem.* **2023**, 38(1), 215818.
2. Bobrovs, R.; Basens, E. E.; Drunka, L.; Kanepe, I.; Matisone, S.; Velins, K. K.; Andrianov, V.; Leitis, G.; **Zelencova-Gopejenko, D.**; Rasina, D.; Jirgensons, A.; Jaudzems, K. Exploring Aspartic Protease Inhibitor Binding to Design Selective Antimalarials. *J. Chem. Inf. Model.* **2022**, 62(13), 3263–3273.
3. Leite, I.; Andrianov, V.; **Zelencova-Gopejenko, D.**; Loza, E.; Kazhoka-Lapsa, I.; Domracheva, I.; Stoyak, M.; Chłopicki, S.; Kalvins, I. Aziridine-2-Carboxylic Acid Derivatives and Its Open-Ring Isomers as a Novel PDIA1 Inhibitors. *Chem. Heterocycl. Compd.* **2021**, 57(11), 1086–1106.
4. Vitkovska, V.; Zogota, R.; Kalnins, T.; **Zelencova, D.**; Suna, E. Aliphatic Chain-Containing Macrocycles as Diazonamide A Analogs. *Chem. Heterocycl. Compd.*, **2020**, 56(5), 586–602.
5. Brangulis, K.; Akopjana, I.; Petrovskis, I.; Kazaks, A.; **Zelencova, D.**; Jekabsons, A.; Jaudzems, K.; Tars, K. BBE31 from the Lyme Disease Agent *Borrelia burgdorferi*, Known to Play an Important Role in Successful Colonization of the Mammalian Host, Shows the Ability to Bind Glutathione. *Biochim. Biophys. Acta - Gen. Subj.*, **2020**, 1864(3), 129499.
6. Czarna, A.; Wang, J.; **Zelencova, D.**; Kildalsen, H.; Seternes, O. M.; Gray, N.; Engh, R. A.; Rothweiler, U. Novel Scaffolds for DYRK1A inhibitors. *J. Med. Chem.*, **2018**, 61(17), 7560–7572.

Author's patents

1. Kalvins, I.; Chłopicki, S.; Andrianov, V.; Stojak, M.; Domracheva, I.; Kanepe-Lapsa, I.; **Zelencova, D.**; Wietrzyk, J.; Turlej, E.; Stachowicz, M.; Jarosz, J.; Milczarek, M.; Kramkowski, K. Aromatic Sulphonamides Derivatives that Inhibits PDI A1, Their Synthesis and Use. WO2021141506A1, **2021**.
2. Chłopicki, S.; Kalvins, I.; Przyborowski, K.; Stojak, M.; Andrianov, V.; Domracheva, I.; Kanepe-Lapsa, I.; **Zelencova, D.**; Wietrzyk, J.; Turlej, E.; Stachowicz, M.; Jarosz, J.; Milczarek, M.; Kramkowski, K. Aromatic Sulphonamides Derivatives that Inhibits PDI A3, Their Synthesis and Use. WO2021141507A1, **2021**.
3. Kalvins, I.; Pyrc, K.; Chłopicki, S.; Andrianov, V.; Domracheva, I.; Kanepe-Lapsa, I.; **Zelencova, D.**; Milewska, A.; Botwina, P. Antiviral Aromatic Sulphonamides Derivatives, Their Method of Synthesis and Use. WO2021141508A1, **2021**.

1. SUMMARY OF LITERATURE REVIEW

The literature review of the Doctoral Thesis summarizes the latest literature on the studied enzymes – BBOX and TMLD, as well as FA transport protein – FABP3. An insight into the physicochemical methods used in this research is provided, such as dynamic light scattering (DLS), thermal shift analysis (TSA), ITC, protein NMR, and molecular dynamics (MD). The summary of the literature review provides information about the examined proteins, which is important for a better understanding of the results.

1.1. BBOX and TMLD enzymes

Acylcarnitines are formed in the organism in an esterification reaction between acyl-CoA and *L*-carnitine mediated by carnitine palmitoyltransferase 1. They are the transport form of FAs and provide FA transport from the cytosol to the mitochondrial matrix, where they undergo β -oxidation [6–8]. The synthesis of acylcarnitines can be significantly slowed down by reducing the bioavailability of *L*-carnitine. The organism can obtain *L*-carnitine from the diet, as well as synthesize it endogenously in four sequential enzymatic reactions (Fig. 1.1) [8, 9]. Two crucial enzymes in this reaction cascade are TMLD (EC 1.14.11.8) and BBOX (EC 1.14.11.1). They catalyse the first and the last reaction, respectively, which involve the stereospecific hydroxylation of the corresponding substrate [TML or γ -butyrobetaine (GBB)] at the β -position (Fig. 1.1). Moreover, the configuration of the new chiral centre of both reaction products [β -hydroxy- ϵ -trimethyl-*L*-lysine (HTML) and *L*-carnitine] is identical with respect to the arrangement of the carboxyl- and trimethylammonium groups [10, 11]. Both enzymes belong to the non-heme Fe(II) and α -ketoglutarate (α KG)-dependent oxygenase family [12–14]. They share 23 % identity in their primary structures making BBOX and TMLD the closest homologs.

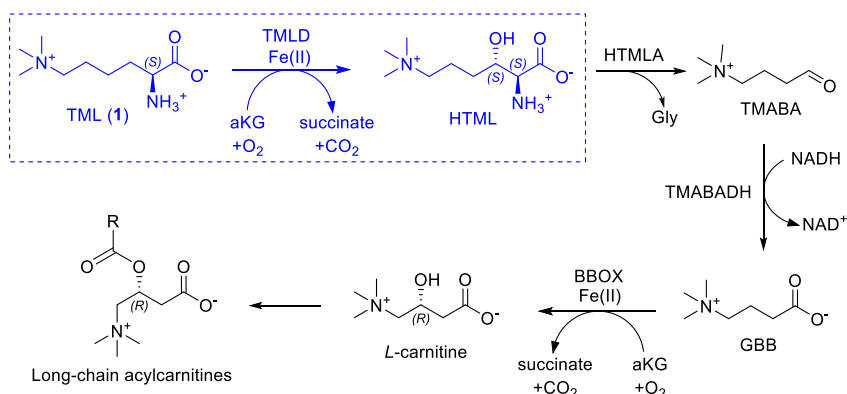


Fig. 1.1. Biosynthesis of *L*-carnitine.

TML: ϵ -trimethyl-*L*-lysine; TMLD: TML dioxygenase; HTML: β -hydroxy-TML; HTMLA: HTML aldolase; TMABA: trimethylaminobutyraldehyde; TMABADH: TMABA dehydrogenase; GBB: γ -butyrobetaine; BBOX: GBB dioxygenase.

Several BBOX crystal structures have been obtained to date, both for the apo-form [15] and for the complexes with various ligands (holo-form) [16–18]. However, all attempts to obtain the experimental structure of TMLD by means of crystallization have been unsuccessful while the size of TMLD is too large to determine the 3D structure by liquid NMR. Thus, an alternative method, mutagenesis, was used to study the active centre of TMLD.

According to 19 newly created human TMLD mutants [19], the importance of the following residues in cofactor or substrate binding was demonstrated:

- 1) Fe(II) chelating residues, the catalytic triad: H242, D244 and H389;
- 2) α KG binding residues: R391 and R398;
- 3) TML trimethylammonium binding residues (i.e., “aromatic cage”): Y217, W221, and Y234;
- 4) TML α -amino and carboxyl group binding residues: D231, N334 and Y404.

Using the obtained data and a homology modelling approach, a model for the active site of TMLD was created (Fig. 1.2), which represents the experimental data with very good confidence [19].

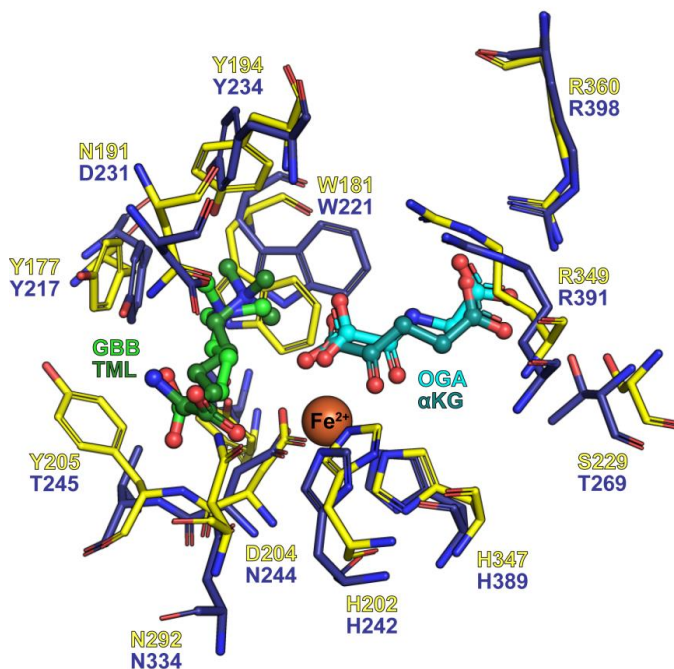


Fig. 1.2. Superposition of the active site of BBOX crystal (PDB ID 4C5W) and TMLD homology model [19].

Residues of BBOX (yellow) and TMLD (dark blue) are shown as tubes with the corresponding naming. Fe(II) is shown as a brown sphere, while *N*-oxalylglycine (OGA) and α KG – as light blue and blue-green balls-and-sticks, respectively. TML is shown as dark green but GBB – as light green balls-and-sticks. Prepared using PyMOL software [20].

1.2. FABP3 transport protein

Heart FABP, also known as H-FABP or FABP3 (UniProt ID P05413 [21]), is one of the most common representatives of FABP found not only in the heart, but also in the kidney, skeletal muscles, aorta, adrenal gland, placenta, brain, testis, ovary, lung, mammary epithelial cells, and stomach tissues [22]. Moreover, it is the only representative of the FABP family found in the heart and red skeletal muscle tissue [23]. FABP3 is a small (14.9 kDa) globular protein that belongs to the lipid-binding protein superfamily. Its main function is the transport of the highly lipophilic FAs in the cytosol, thus regulating intracellular functions such as membrane phospholipid synthesis, lipid metabolism, and mitochondrial β -oxidation [22, 24]. The protein structure consists of a pair of five stranded antiparallel β -sheets, which form a barrel β_A - β_J closed by two short α -helices: α_I and α_{II} . This results in a large internal cavity capable of binding one long-chain FA (Fig. 1.3). The adjacent antiparallel β -strands, β_D and β_E , are too far apart and are unable to form interstrand hydrogen bonds creating the so-called “gap” (Fig. 1.3, dark yellow region). In the binding site, the long-chain FAs adopt a U-shaped conformation and bind to R127 and Y129 with their carboxyl group. Meanwhile, the alkyl chain binds to the lipophilic residues that form the opening of the binding site (portal) – α_{II} helix and loops between C–E and E–F β -strands (Fig. 1.3, pink region) – and the cavity of the binding site [25–27].

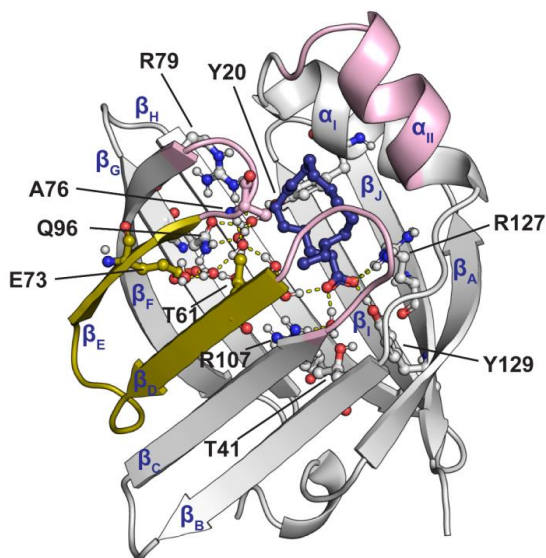


Fig. 1.3. Structure of FABP3 protein in complex with palmitate (C16:0) and internal water molecules (PDB ID 3WVM).

Protein structure is represented as grey ribbons together with the bound ligand (dark blue balls-and-sticks) and water molecules (red spheres). The Ligand entry portal and gap region between β_D and β_E β -strands are shown in pink and dark yellow, respectively. Hydrogen bonds are shown as yellow dashed lines.

Prepared using PyMOL software [20].

2. SUMMARY OF RESULTS AND DISCUSSION

2.1. Design of the TMLD mimetics based on BBOX

2.1.1. Protocol development for the MD simulations of *in silico* BBOX mutants

Analysis of the active site of BBOX revealed 18 amino acids that are in direct contact with BBOX substrate, GBB, and cofactors, Fe(II)/ α KG, and ensure their recognition and binding: Y177, W181, V183, N191, A193, Y194, L199, H202, D204, Y205, P206, N292, T295, H347, R349, R360, L362, and Y366. In TMLD, the region around the Fe(II)/ α KG binding site is conserved by 89 %, while the substrate binding site is conserved only by 64 %. Most probably, the differences observed in the residues of the active site of the enzyme, N191D, Y205T, P206T, and T295D, provide recognition of the TML α -amino group.

Based on the mutagenesis of TMLD [19] and sequence analysis of BBOX/TMLD, the following four *in silico* BBOX mutants were created:

- 1) BBOX-2m: N191D, T295D;
- 2) BBOX-4m: N191D, Y205T, P206T, T295D;
- 3) BBOX-5m: V183F, N191D, Y205T, P206T, T295D;
- 4) BBOX-7m: Q182Y, V183F, Q184T, N191D, Y205T, P206T, T295D.

At first, the stability of the newly created BBOX mutants was tested *in silico* using MD simulations. For this purpose, the MD protocol was developed based on BBOX (PDB ID 3O2G). Both BBOX and TMLD are metalloproteins. Thus, additional force field restraint potentials were introduced in the simulation to maintain the tetragonal bipyramid of Fe(II), as classical molecular mechanics cannot reproduce the charge distribution in such systems. The best results were achieved by freezing all 12 dihedrals of the bipyramid. The analysis of the enzyme-ligand contact network showed that the freezing of the tetragonal bipyramid did not affect the formation of the interactions between BBOX, α KG, and GBB.

2.1.2. MD simulations of the BBOX mutants

The stability of the BBOX mutant complexes with GBB or TML was tested in 100 ns long MD simulations utilizing root mean square deviation (RMSD), root mean square fluctuation (RMSF) and solvent accessible surface area (SASA) analysis as the resultative indicators. In some simulations, substrate (GBB or TML) dissociation from the enzyme active site was observed. In the case of the most unstable complexes (e.g., BBOX-4m-GBB), such a dissociation occurred already at the beginning of the simulation (after ~ 10–20 ns). As a result, it was shown that the newly generated BBOX mutants bind TML much better than GBB.

Based on the analysis of the MD data for four different BBOX mutants, it was concluded that the most stable complexes are the ones of TML with BBOX-2m and BBOX-4m. Thus, these two forms of the enzyme were further tested experimentally.

2.1.3. Production of *in vitro* BBOX-4m and 2m mutants. Enzymatic tests

2.1.3.1. Production of BBOX-4m

Introducing four mutations (N191D, Y205T, P206T, and T295D) into the active site of BBOX made it as unstable as the TMLD enzyme. As a result, active BBOX-4m enzyme could be obtained only in the form of a fusion¹ protein with maltose-binding protein (MBP). The expression was performed in *E. Coli* BL21-AI cells in the presence of the molecular chaperones GroEL/ES, similarly to TMLD [28]. Expression tests revealed that the formation of soluble MBP-BBOX-4m could be improved by reducing the induction temperature from 37 to 16 °C. Thus, the following final yields were obtained for MBP-BBOX-4m:

- 1) 37 °C: ~ 0.3 mg/L 2xYT medium;
- 2) 16 °C: ~ 1.9 mg/L 2xYT medium.

2.1.3.2. Production of BBOX-2m

On the other hand, BBOX-2m with N191D and T295D mutations turned out to be more stable than BBOX-4m. However, it was also obtained only as MBP-BBOX-2m fusion protein with the following final yields:

- 1) 37 °C: ~ 2.4 mg/L 2xYT medium;
- 2) 16 °C: ~ 6.6 mg/L 2xYT medium.

As it can be seen, expression at 37 °C resulted in up to 8-times more and at 16 °C – 3.5 times more of 2-fold mutant than 4-fold mutant. The obtained experimental data indicate that Y205T and P206T mutations strongly destabilize the BBOX structure, resulting in significantly reduced enzyme yields. It is possible that additional mutations in the second ligand coordination sphere (>4 Å apart) would be necessary to compensate for the increased mobility in the active site caused by these mutations. However, a larger number of mutations can greatly alter the BBOX structure, making the created mimetics uninformative.

2.1.3.3. Enzymatic tests of MBP-BBOX-4m and MBP-BBOX-2m

The obtained activity of the BBOX mutants was evaluated by performing enzymatic reactions and monitoring them by 1D ¹H NMR spectroscopy. 200 μM TML, GBB, or δ-trimethyl-L-ornithine were used as substrates. Initially, 3.0 μM enzyme was used for the reaction. Unfortunately, no changes in the ligand chemical shifts or signal intensities were observed in any sample. This indicates that no rapid conversion of substrate or αKG occurred in any of the reaction mixtures.

On the other hand, 4–6-fold increase in the intensity of the succinate signal was observed in comparison to the reference spectrum at a higher enzyme concentration. Moreover, when the

¹ fusion or chimeric protein – a protein consisting of two or more covalently linked proteins/protein domains that do not occur in nature.

concentration was increased to 19.8 μM , a significant line broadening of the $(\text{CH}_3)_3\text{N}^+$ signal was observed in the spectrum (Fig. 2.1). This effect becomes more pronounced with increasing the enzyme concentration to 43.6 μM (1 : 4.6 enzyme-ligand ratio). Values of the signal widths depending on the enzyme concentration are summarized in Table 2.1. A comparison of the enzymatic reaction spectra of all three ligands and the line-broadening data reveal that MBP-BBOX-2m has a preference for the substrates containing an α -amino group. In order to test the functionality of the enzyme, one should try to perform the enzymatic reaction with α -amino-GBB, which is a BBOX substrate from *Pseudomonas sp.* [29].

Overall, despite convincing MD data, it seems that more mutations are needed to change the substrate selectivity of the BBOX active site to “teach” it to process TML. Most likely, the lengths of the $\beta\text{I}/\beta\text{II}$, $\beta\text{II}/\beta\text{III}$, and $\beta\text{III}/\beta\text{IV}$ loops that cover the active site in the double-stranded β -helix (DSBH) structure motif and participate in the substrate binding should be increased.

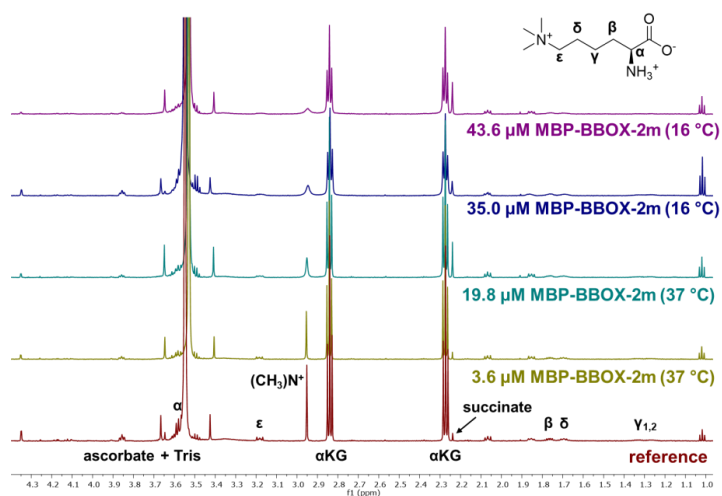


Fig. 2.1. 1D ^1H NMR spectra of the enzymatic reaction of MBP-BBOX-2m with TML.

Spectrum in red – reference spectrum of the enzymatic reaction mixture with 200 μM TML without addition of the enzyme. Spectrum in yellow – 200 μM TML with 3.6 μM MBP-BBOX-2m (expressed at 37 $^\circ\text{C}$) after 1 h incubation at 37 $^\circ\text{C}$. Spectrum in cyan – 200 μM TML with 19.8 μM MBP-BBOX-2m (expressed at 37 $^\circ\text{C}$) after 1 h incubation at 37 $^\circ\text{C}$. Spectrum in dark blue – 200 μM TML with 35.0 μM MBP-BBOX-2m (expressed at 16 $^\circ\text{C}$) after 1 h incubation at 37 $^\circ\text{C}$. Spectrum in violet – 200 μM TML with 43.6 μM MBP-BBOX-2m (expressed at 16 $^\circ\text{C}$) after 1 h incubation at 37 $^\circ\text{C}$.

Table 2.1

Dependency of the changes in the linewidth of the $(\text{CH}_3)_3\text{N}^+$ group signal on the concentration of MBP-BBOX-2m

Enzyme conc., μM	TML, ppm	GBB, ppm	δ -trimethyl-L-ornithine, ppm
0	1.80	1.64	2.0
3.6	1.84	1.71	n/d
19.8	5.56	2.67	n/d
35.0	12.11	n/d	13.08
43.6	17.27	4.46	n/d

n/d – no data

2.2. Design of the TMLD model by artificial intelligence (AlphaFold)

The model of human full-length TMLD structure is available in AlphaFold [30, 31] database along with the model confidence scores indicating high confidence of the structural and catalytic domains of the model. The calculated position errors are displayed as a 2D plot where the position errors are indicated by a colour gradient ranging from dark blue to yellow, where darker regions correspond to the smallest position errors. Analysing the expected position errors of the 15 residues in the active centre of the TMLD model, a new 2D plot (Fig. 2.2) was created using a *Python v.3* script written by the author. As one can see, the most confident region is around the Fe(II)/ α KG binding site (H242, D244, H389, and R391, R398, respectively). Two regions are formed at the binding site of TML, one with the highest (Y217, W221, T245, T269, N334, D337, and Y404), and the other one with the lowest (F223, D231, and Y234) confidence. Nevertheless, the AlphaFold model was more stable during MD simulation than the homology model of the TMLD enzyme [32] (Fig. 2.3).

Overall, the obtained TMLD model using artificial neural networks appears to be more stable and reliable than previously created homology models and is in a good agreement with the experimental data from TMLD mutants [33]. Based on the obtained results, the AlphaFold model of TMLD was further used for the modelling of the enzyme-ligand complexes with the aim of rationalizing the obtained experimental data and determining structure-activity relationships.

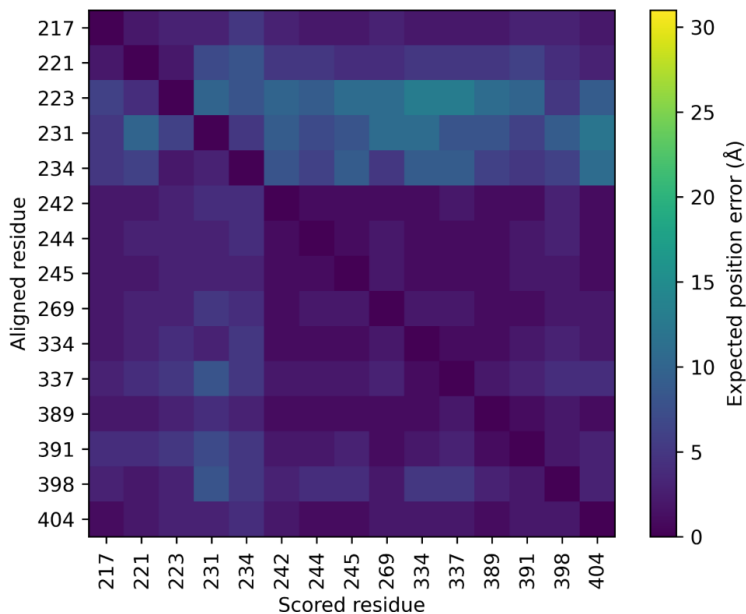


Fig. 2.2. Expected position errors for the predicted residues in the active site of TMLD that participate in the ligand binding at residue x when the predicted and true structures are aligned on residue y , calculated by AlphaFold. Dark blue represents no error while yellow indicates high error regions.

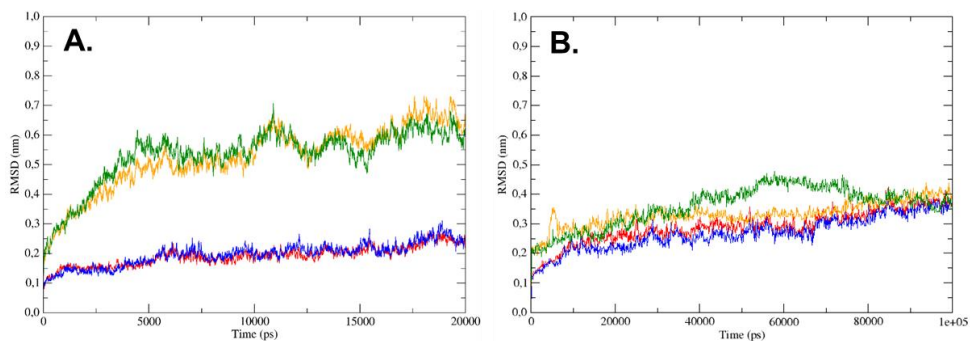


Fig. 2.3. Changes in RMSD during MD simulation of BBOX (PDB ID 3O2G) and TMLD models.

A. Comparison of RMSD during 20 ns long MD simulation of BBOX (PDB ID 3O2G) and homology model of TMLD that was prepared using *Prime* software [32]. **B.** Comparison of RMSD during 100 ns long MD simulation of BBOX (PDB ID 3O2G) and TMLD model created by AlphaFold. RMSD of BBOX chain A – in red; BBOX chain B – in blue; RMSD of TMLD chain A – in yellow; RMSD of TMLD chain B – in green.

2.3. Optimization of large-scale production of active MBP-TMLD

2.3.1. Optimization of expression and purification conditions

2.3.1.1. Tests of the expression media

The impact of four *E. Coli* expression media on yields and formation of aggregates of MBP-TMLD were evaluated for optimization of its final yield:

- 1) LB (Lysogeny broth) – standard expression medium for bacteria;
- 2) 2xYT – enriched medium, where the amount of tryptone and yeast is doubled in comparison to LB;
- 3) 2xYT medium with 100 μ M Zn(II) supplement that could enhance the formation of a Zn(II) finger motif in the *N*-terminal structural domain;
- 4) TB (Terrific broth) – highly enriched medium with trace element² additive.

Table 2.2

Final yield of MBP-TMLD upon varying of *E. Coli* cultivation medium

	LB	2xYT	2xYT + Zn(II)	TB
Amount of cells	4.1 g/L	6.0 g/L	6.2 g/L	5.5 g/L
Total amount of enzyme after MBPTrap TM	9.7 mg/L	16.5 mg/L	15.6 mg/L	14.2 mg/L
	2.4 mg/g	2.8 mg/g	2.5 mg/g	2.6 mg/g
Amount of dimer after SEC ³	0.80 mg/g	1.16 mg/g	0.93 mg/g	0.57 mg/g

² The composition of the trace element additive: 50 μ M FeCl₃, 20 μ M CaCl₂, 10 μ M MnCl₂ and ZnSO₄, 2 μ M CoCl₂, CuCl₂, NiCl₂, Na₂SeO₃, and H₃BO₃.

³ SEC – size-exclusion chromatography or gel filtration.

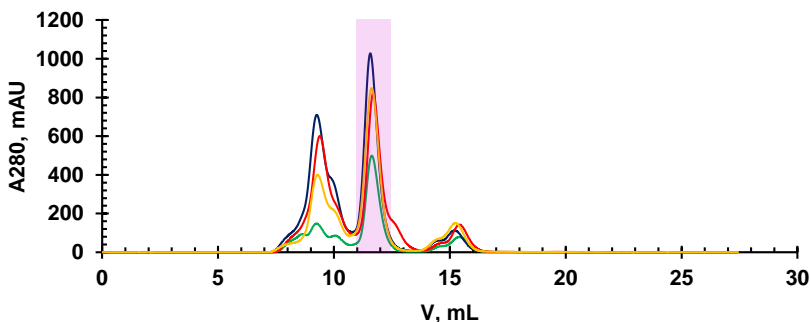


Fig. 2.4. Superposition of SEC chromatograms of the MBP-TMLD enzyme from Superdex™ 200 Increase 10/300 GL column.

MBP-TMLD expressed in: LB medium – green curve; 2xYT medium – dark blue curve; 2xYT medium with Zn(II) supplement – red curve; TB medium – yellow curve. The pink region highlights the peak corresponding to the enzyme dimer (~ 174 kDa).

The obtained data (Table 2.2 and Fig. 2.4) reveal that rich TB medium promotes the formation of aggregates, which is most likely due to too fast cell growth that negatively affected the folding of MBP-TMLD. Thus, the solubility of the enzyme decreased and the amount of aggregates increased. The addition of Zn(II) to the 2xYT medium did not affect the final yield. However, an additional shoulder of the dimer peak (Fig. 2.4, 12.5–13.5 mL) can be seen in the SEC chromatogram of MBP-TMLD, which probably indicates the formation of a new dimer conformation. The enzyme yields in the LB medium were significantly lower than in 2xYT and TB media as well. As a result, further enzyme production was carried out in the classic 2xYT medium.

2.3.1.2. Search for stabilizing conditions using the TSA method

Several stabilizing conditions that increase the melting (denaturation) temperature of MBP-TMLD and stabilize the enzyme were found by the TSA method. The enzyme was maximally stable at pH 7.0 and 7.5, which is at least one unit higher than its pI 6.08, and the least stable at pH 4.5 and 10.0, which are very extreme conditions. The enzyme also showed sufficient stability in Tris buffer at pH 8.0 in comparison to MES at pH 6.0. Increasing the concentration of NaCl in the sample did not cause any significant changes, however, the salt concentration that stabilized the enzyme was in the range of 200–500 mM, while it slightly destabilized the enzyme at 1000 mM concentration. The best results were obtained for the following stabilizing additives: 10 % glycerol, sugars (*D*-trehalose, *D*-sucrose, and *L*-arabinose), and amino acid (*L*-Arg and *L*-Glu) additives. Thus, PIPES, HEPES, or Tris buffers at pH 7.0–8.0 should be used in the experiments together with NaCl or KCl at concentrations <1000 mM.

2.3.1.3. Tests of stabilizing additives during the sonication of the cells

Similarly to the BBOX mutants, lowering the expression temperature from 37 to 20 °C improved the folding of MBP-TMLD, which resulted in an approximately twofold increase in

the soluble protein (Fig. 2.5, control samples 1–6). According to the TSA analysis, the effect of the selected stabilizing additives during sonication on enzyme activity and final yield was evaluated. As can be seen from the SDS-PAGE gel, the addition of 10 % (v/v) glycerol (Fig. 2.5, 7, and 8) minimally increased, but the addition of 0.7 M *D*-trehalose (Fig. 2.5, 10, and 11) significantly improved the amount of soluble enzyme. The maximal yield was obtained for the sample expressed at 20 °C. The comparison of the amounts of aggregates and MBP-TMLD dimer after purification on a SEC column (Fig. 2.6) reveals the increase in the soluble enzyme portion by ~ 70 % in the sample expressed at 20 °C and sonicated in the presence of *D*-trehalose than in the sample that was sonicated without the additive. Moreover, the sample purified in the presence of *D*-trehalose showed an activity improvement from 40–50 % to 80–85 % (determined in the ITC experiment by the stoichiometry value). The obtained results were described in the author’s publication [34].

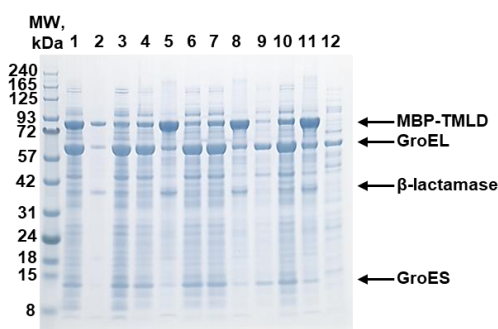


Fig. 2.5. SDS-PAGE analysis of the optimization of expression and purification conditions of MBP-TMLD at 20 and 37 °C.

Control samples 1–3 and 4–12 correspond to enzyme portions expressed at 20 and 37 °C, respectively. Control samples 1–6 – enzyme samples sonicated in lysis buffer without additives; 7–9 – enzyme samples sonicated in lysis buffer with 10 % (v/v) glycerol; 10–12 – enzyme samples sonicated in lysis buffer with 0.7 M *D*-trehalose. Control samples 1, 4, 7, and 10 – supernatant containing soluble fraction of enzyme; 3, 5, 8, and 11 – cell pellets containing insoluble fraction of enzyme; 2, 6, 9, and 12 – flow-through from the HisTrap™ column washing.

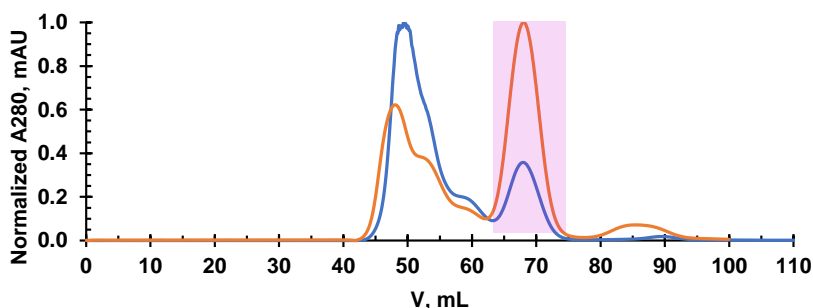


Fig. 2.6. Superposition of normalized SEC chromatograms of the MBP-TMLD enzyme from *HiLoad 16/600 Superdex™ 200pg* column.

MBP-TMLD sonicated without (blue curve) and with (orange curve) the addition of 0.7 M *D*-trehalose stabilizing additive. The pink region highlights the peak corresponding to the enzyme dimer (~ 174 kDa). Curves normalized by absorption at 280 nm (A280).

2.3.2. The effect of EDTA on MBP-TMLD

A strong chelating agent for metal “stripping” from the proteins – ethylenediaminetetraacetic acid (EDTA) was applied to ensure that no metal ions remained in the active site of MBP-TMLD after purification from *E. Coli*, which could reduce its catalytic activity. Enzyme titration with EDTA did not show any significant heat effect. A similar effect was also observed in the ITC experiment where MBP-TMLD was titrated with TML without adding the cofactors or in complex with *N*-oxalylglycine (OGA⁴) only (Fig. 2.7, A). Furthermore, incubation of the enzyme with EDTA before SEC chromatography neither affects the enzyme’s conformation nor its activity (determined by the ITC experiment by stoichiometry, Fig. 2.7, B). Overall, it can be seen that the active site of MBP-TMLD is not blocked by other metal ions and effective substrate binding occurs only in the presence of both cofactors Fe(II)/ α KG or their isosteres. The obtained data were described in the author’s publication [34].

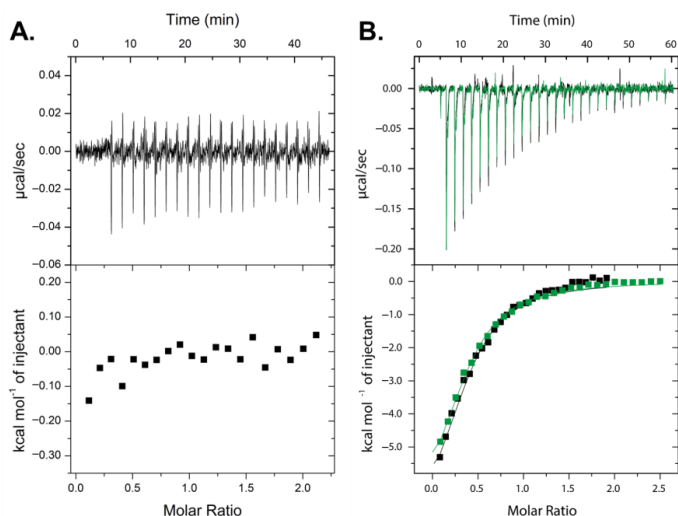


Fig. 2.7. ITC titration data for MBP-TMLD at 25 °C.

A. MBP-TMLD in complex with OGA (2-fold excess) titrated with TML. **B.** MBP-TMLD purified without (black) and with (green) pre-treatment with EDTA in complex with Zn(II)/OGA (2-fold excess) titrated with TML.

2.4. Development of the ITC assay for MBP-TMLD enzyme

MBP-TMLD requires the following cofactors for the enzymatic activity: Fe(II) and α KG, which in turn ensure an instantaneous enzymatic reaction. Therefore, to determine the heat effect of ligand binding, natural cofactors must be replaced with isosteres that fulfil a similar structural function but block the enzymatic reaction. OGA – the isostere of α KG is well known and widely used in BBOX crystallization and ITC studies [16, 35]. On the contrary, various

⁴ OGA – α KG isostere.

metal ions can serve as Fe(II) isosteres sharing sizes similar to iron and the ability to form six coordination bonds. Here, the following nine ions were tested: Ni(II), Zn(II), Mn(II), Fe(III), Cr(II), Co(II), Cu(II), Mg(II), and Ca(II). Interestingly, a combination of Ni(II)/OGA provided the best results in the case of BBOX ITC titration experiment [35], whereas it turned out to be inactive in the MBP-TMLD titration with TML. The only metals that showed significant changes in heat effect in the titration experiment with TML in combination with OGA were Co(II) and Zn(II). However, the heat released in the case of Zn(II) was at least 4-fold higher. Thus, Zn(II) was used as the Fe(II) isostere in the subsequent experiments.

In addition, the necessary amounts of the cofactors were tested to fully saturate the active site of MBP-TMLD and to provide the highest stoichiometry, N . The results are shown in Fig. 2.8. An excess of ~ 20 % of cofactors already allowed to achieve $N \sim 0.92$ (Fig. 2.8 A). In contrast, 2-fold excess gives only a minimal improvement, $N \sim 0.92$ (Fig. 2.8, B), while 4-fold excess caused an unexpected decrease in the stoichiometry to $N \sim 0.24$ (Fig. 2.8 C). It is possible that such a decrease in stoichiometry may be related to the increased ability of Zn(II) ions to cause protein precipitation. Thus, Zn(II)/OGA were used as the cofactors that were added to the enzyme in the 2-fold excess just before the experiment in the subsequent ITC titrations with the MBP-TMLD enzyme.

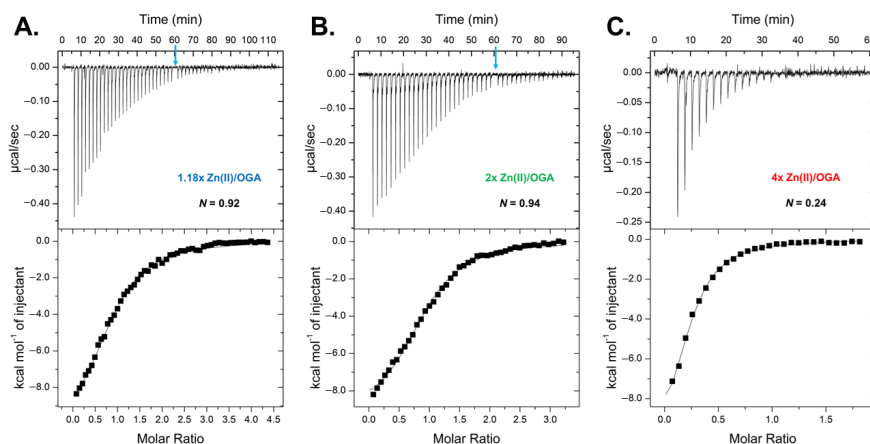


Fig. 2.8. ITC titration data for MBP-TMLD in complex with Zn(II)/OGA titrated with TML varying concentrations of the cofactors at 25 °C.

MBP-TMLD in complex with Zn(II)/OGA **A.** 1.18-fold excess; **B.** 2-fold excess; **C.** 4-fold excess. Light blue arrow points to the syringe refill.

2.5. Study of structure-activity relationship of TMLD

2.5.1. Studies of binding relationships of TML analogues

The developed ITC assay was used to test TML and 11 TML analogues that were synthesised at the Latvian Institute of Organic Synthesis (LIOS) (Table 2.3). Ligands were designed by varying the aliphatic chain length (compounds **2**, **3**), introducing substituents at the

ϵ -N nitrogen atom (compounds **4–7**) or the α -N nitrogen atom (compound **8**). Several *D*-isomers **9–11** and compound **12** lacking the α -amino group were synthesized as negative controls (Fig. 2.9). The synthetic procedures were described in the author's publication [34].

Table 2.3

ITC results and NMR conversion rates of MBP-TMLD interaction/reaction with TML and its analogues at 25 °C

#	Compounds ^a	K_D , μM	ΔG , $\text{kcal}\cdot\text{mol}^{-1}$	ΔH , $\text{kcal}\cdot\text{mol}^{-1}$	$-T\Delta S$, $\text{kcal}\cdot\text{mol}^{-1}$	Amount of H ^b , %	S/H ^c ratio
1		5.78 ± 0.06	-7.15 ± 0.01	-5.48 ± 0.08	-1.66 ± 0.08	97 ± 1	1.3 ± 0.3
2		7.6 ± 0.3	-6.9 ± 0.1	-4.5 ± 0.4	-2.5 ± 0.5	28 ± 5	3.1 ± 0.5
3		25 ± 1	-6.28 ± 0.03	-1.4 ± 0.2	-4.9 ± 0.2	30 ± 2	2.9 ± 0.2
4		6.0 ± 0.1	-7.12 ± 0.01	-6.37 ± 0.05	-0.75 ± 0.06	83 ± 2	2.1 ± 0.3
5		9.2 ± 1.6	-6.9 ± 0.1	-1.4 ± 0.2	-5.5 ± 0.3	25 ± 6	3.4 ± 0.4
6		11.3 ± 0.2	-6.75 ± 0.01	-5.6 ± 0.3	-1.2 ± 0.3	51 ± 3	2.4 ± 0.1
7		16.4 ± 0.2	-6.52 ± 0.03	-0.6 ± 0.1	-5.9 ± 0.1	39 ± 3	2.4 ± 0.1
8		–	–	–	–	12 ± 3	3.9 ± 0.8

^a Compounds **9–15** (Fig. 2.9) neither show binding heat effects nor conversion rates in the enzymatic assay.

^b H – hydroxylated substrate.

^c S/H – ratio of succinate formation to hydroxylation.

Despite the variability in the chain length, all *D*-isomers [*D*-TML (**9**), δ -trimethyl-*D*-ornithine (**10**), and ζ -trimethyl-*D*-homocysteine (**11**)], as well as the ϵ -trimethylamino-hexanoate (**12**) did not interact with MBP-TMLD. Similarly, no binding was detected in the ITC experiment for α -*N*-isobutyryl- ϵ -trimethyllysine (**8**). These data confirm the requirement of the unhindered primary amino group with *L*-stereochemistry for the high-affinity binding to the enzyme.

In the case of TML, the determined K_D value was 5.78 μM (Table 2.3). The thermodynamic binding profile shows both binding-favourable enthalpy (ΔH) and entropy ($-T\Delta S$) components (Fig. 2.10 A). The absolute value of ΔH is 3.3-fold larger than that of the $-T\Delta S$ indicating a mainly enthalpy-driven binding mechanism as well. Similar binding was observed for

compounds **4** and **6**. On the other hand, compounds **3**, **5**, and **7** had different thermodynamic binding profile (Fig. 2.10 C) with dominating entropic contribution and smaller ΔH (by the absolute value). Most probably, such a mechanism reveals weakening of the electrostatic contact network between the enzyme and the ligand as well as large binding-favourable rearrangement in the active site. This binding process is entropy-driven.

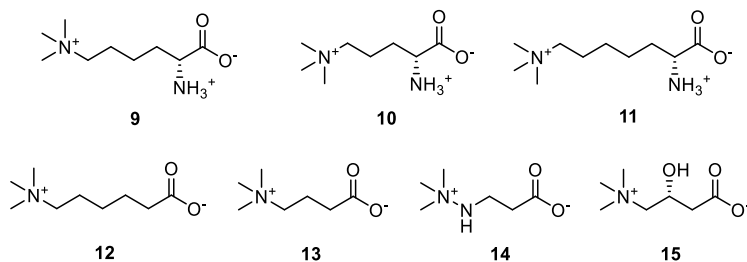


Fig. 2.9. TML analogues (**9–12**) and BBOX binders (**13–15**) that are neither substrates nor binders of TMLD.

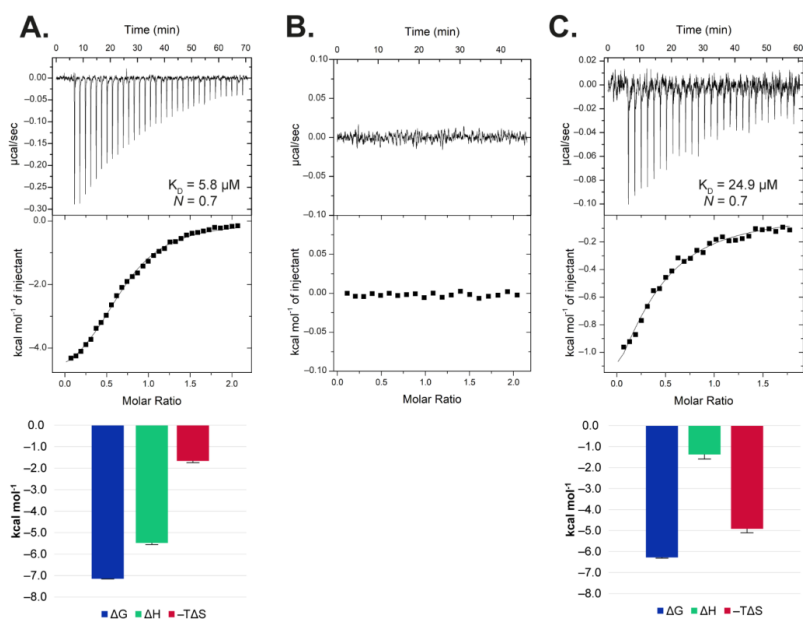


Fig. 2.10. ITC titration curves (top) and graphical representation of the thermodynamic binding parameters (bottom) of MBP-TMLD.

A. MBP-TMLD saturated with Zn(II)/OGA and titrated with TML. **B.** MBP-TMLD saturated with Zn(II)/OGA and titrated with *D*-TML. **C.** MBP-TMLD saturated with Zn(II)/OGA and titrated with ζ -trimethyl-*L*-homolysine. All experiments were performed at 25 °C.

Compounds with the substituents at the position of the ϵ -*N*-ammonium group form the following list based on their binding affinities: Me ~ Et > *n*-Pr > *i*-Pr > *n*-Bu. As one can see, the affinity reduced with the increase of the substituent length. Interestingly, in the case of

BBOX, γ -(dimethylethylammonio)butyrate (ethyl-GBB) showed the K_D value of one order of magnitude lower than that of the native substrate (Table 2.4). On the contrary, ethyl-TML [ϵ -dimethylethyl-*L*-lysine (**4**)] had a high binding affinity similar to TML in the case of TMLD (Table 2.3).

Table 2.4

Comparison of novel substrates of TMLD [34] with known substrates of BBOX [35]

#	TMLD	BBOX	BBOX PDB ID	BBOX IC ₅₀ , μ M	BBOX K_D , μ M
1			3O2G [16]	x	4.9 \pm 0.2
	no analogues		3MS5 [16]	34–62	24 \pm 4
4			4C5W [35]	3.3 \pm 1.8	46 \pm 10
5			n/d	>1000	n/d
6			n/d	5.7 \pm 1.6	n/d
7			n/d	>1000	n/d

n/d – Experimental data for the BBOX enzyme were not available.

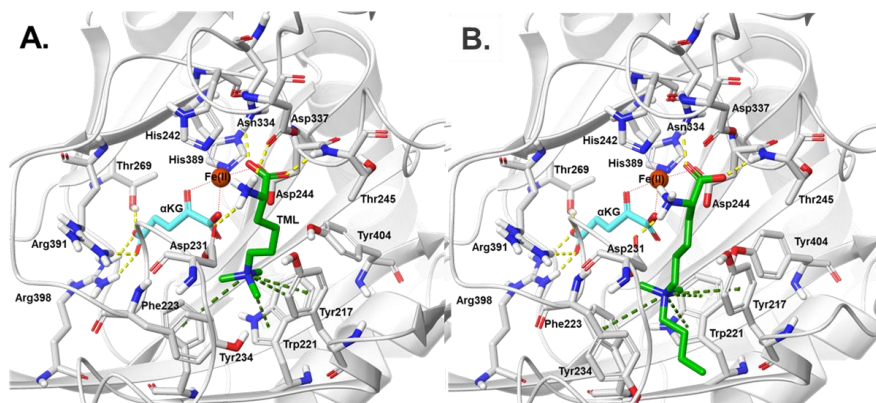


Fig. 2.11. Models of the TMLD active site prepared by IFD with different ligands, showing surrounding residues and cofactors. **A.** TML (**1**) and **B.** ϵ -dimethylbutyl-*L*-lysine (**7**).

Residues are shown in grey tubes. Cofactors: Fe(II) are shown as a brown sphere and α KG in cyan tubes. Ligands are shown in green tubes. Hydrogen bonds are shown in yellow and cation- π stacking – in green dashed lines. Non-polar hydrogens are omitted.

Modelling data reveal that compounds **1**, **4**, and **6** have a highly similar position in the active site (e.g., Fig. 2.11 A) with no penalties for the bioactive conformation. On the other hand, compounds **5** and **7** had values of ΔH close to zero indicating an entropy-driven binding mechanism, similar to compound **3**. These results suggest that the introduction of longer *n*-alkyl chains in the quaternary amino group as well as elongation of the alkyl chain disrupts the substrate-like binding mode of the compounds in the active site of the MBP-TMLD. Modelling data (Fig. 2.11 B) show weakening of the electrostatic contact network and rearrangement of the “aromatic cage” residues. These data are in a good agreement with IC_{50} values for the BBOX enzyme (Table 2.4), where Et- and *i*-Pr substituents provide similar and low IC_{50} values (working as the competitive inhibitors), while *n*-Pr and *n*-Bu gave high IC_{50} values (not inhibitors, did not affect the hydroxylation reaction). IC_{50} values were not disclosed for TMLD in order to be able to include these data in the upcoming patent application.

Next, enzymatic conversion rates of compounds **1–12** were examined for better characterization of the investigated compounds. The enzymatic reaction was monitored by 1D 1H NMR spectroscopy similarly to the approach reported by Al Temimi *et al.* [36]. Fig. 2.12 shows an example of the complete hydroxylation of the starting material (TML) to 2*S*,3*S*-HTML, as can be observed from the up-field shifts of the corresponding signals. The substrate conversion in the enzymatic reaction was quantified by the $(CH_3)_2-3N^+$ group that appears in the spectrum as an isolated singlet at 3.0–3.1 ppm. In addition, the ratios of succinate formation over hydroxylation (S/H) were evaluated. The results are summarized in Table 2.3.

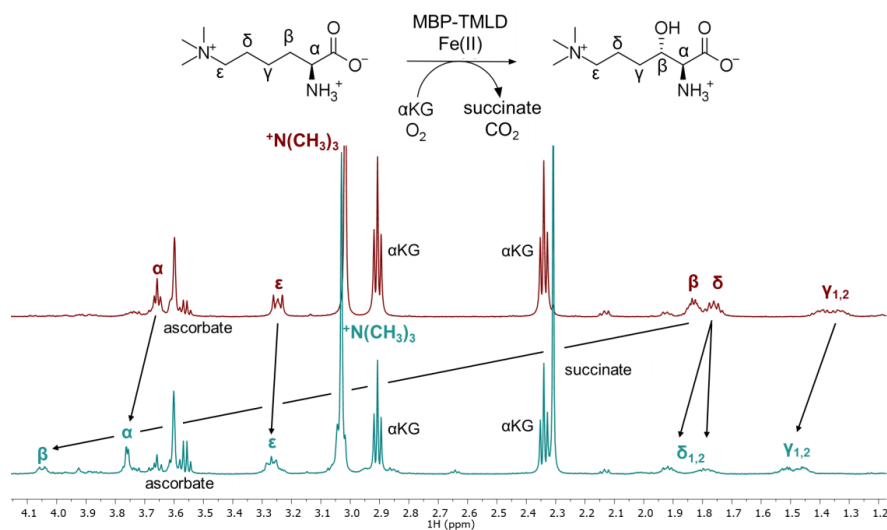


Fig. 2.12. 1D 1H NMR spectra of the enzymatic reaction of MBP-TMLD with TML.

The spectra in red and cyan correspond to the mixture without and with MBP-TMLD, respectively, after incubation at 37 °C for 30 min.

Compounds **9–12** did not show any binding heat effect in the ITC assay and did not work as the substrates of MBP-TMLD, so they were not processed in the enzymatic reaction. The increased production of the succinate was not determined in these samples as well.

Unexpectedly, the enzymatic reaction of **8** yielded 12 % of hydroxylated reaction product linked to a 4-fold larger formation of succinate, which indicates uncoupled turnover of α KG. According to this observation, one can assume that compound **8** can occupy the active site of MBP-TMLD, but the enzymatic reaction is significantly slowed by the introduction of the amide group instead of the α -amino group. In all cases, except the TML hydroxylation, the enzymatic reaction with the analogues of the endogenous substrate showed the stimulation of the α KG turnover yielding 2.1–3.9-fold increase in the S/H ratio. This may indicate that compounds **2–7** can occupy the active site of TMLD but less frequently adopt reactive conformation as manifested by the low hydroxylation yields.

Similarly to the ITC experiments, two groups can be distinguished based on the amount of the hydroxylated product. One group is formed from the compounds **2, 3, 5, and 7**, which were hydroxylated for 25–39 %. Compound **8** with a conversion of 12 % can also be included in this group. The second group consists of TML and compounds **4, 6**, which were hydroxylated for 97 %, 83 %, and 51 %, respectively. The latter were the only three compounds with significant values of ΔH component that share similar enthalpy-driven binding mechanism. Thus, one can conclude that ITC binding mechanism reflects the ability of the potential substrates of TMLD to be hydroxylated and it can be used to predict conversion rates and *vice versa*. Furthermore, uncoupling of the α KG turnover from the hydroxylation indicates that such compounds have prolonged occupancy in the active site of the enzyme without the formation of the reaction product. Such compounds may be used for the *de novo* TMLD inhibitor design due to longer residence times. The obtained data were described in the author's publication [34]. All figures of the ITC and enzymatic reaction experiments are available in the supplementary material of the publication.

2.5.2. Development of the pharmacophore model

The pharmacophore model was developed based on the obtained ITC and NMR experimental data. As a result, geometric constraints were created, which include three pharmacophores: two positive and one negative centre. Additional geometric constraints were not used in the first model (Fig. 2.13 A) and the studied ligands were fitted to the model based solely on the distances between charged centres (Fig. 2.13 B).

On the other hand, additional steric hindrances were introduced in the form of excluded volumes in the second model (Fig. 2.14 A). These are the forbidden zones where the ligands cannot be located. The first model could not distinguish *L*- and *D*-isomers due to the free rotation of the aliphatic chain (Fig. 2.13 C, D). However, the placement of the β -CH₂ group indicates that *D*-isomer adopts unreactive conformation. The excluded volumes in the second model successfully reproduced the spatial constraints of the enzyme active centre and successfully filtered out all *D*-isomers. The comparison of the calculated Phase Screen Score and experimental ΔG values for both models showed a linear correlation with $R^2 = 0.83$ and 0.92 for the first and the second models, respectively. The second model (Fig. 2.14) provided a better fit between experimental and theoretical data and it did not show any false positive selection of *D*-isomers as it was observed in the first model. However, both models were trained specifically

on the TML analogues with relatively high affinities. In order to improve the pharmacophore model, a wider range of ligands with more diverse structures and activities should be used.

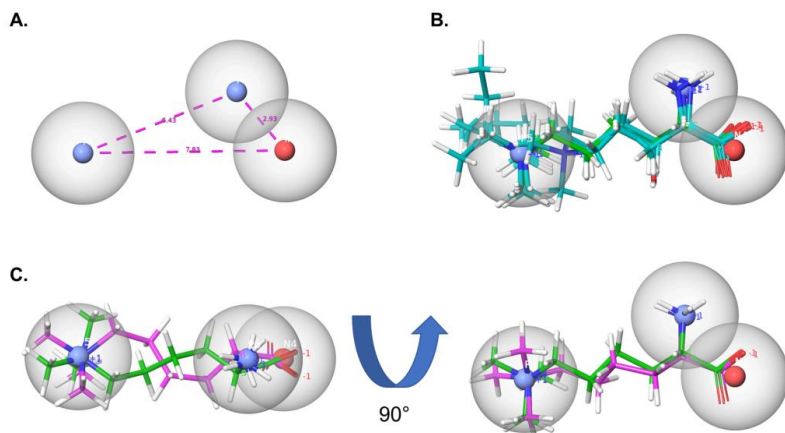


Fig. 2.13. The first pharmacophore model without excluded volumes created from TML and its analogues based on the binding affinities determined by ITC.

A. Pharmacophore model with specified geometric constraints. **B.** Ligand alignment with the pharmacophore model. TML – in green and its analogues (including HTML) – in cyan. **C.** TML (green) and *D*-TML (pink) overlay with the pharmacophore model shown from two viewpoints. Blue spheres – positively charged centres; red sphere – negatively charged centre; grey spheres – tolerance radius around the charged centre.

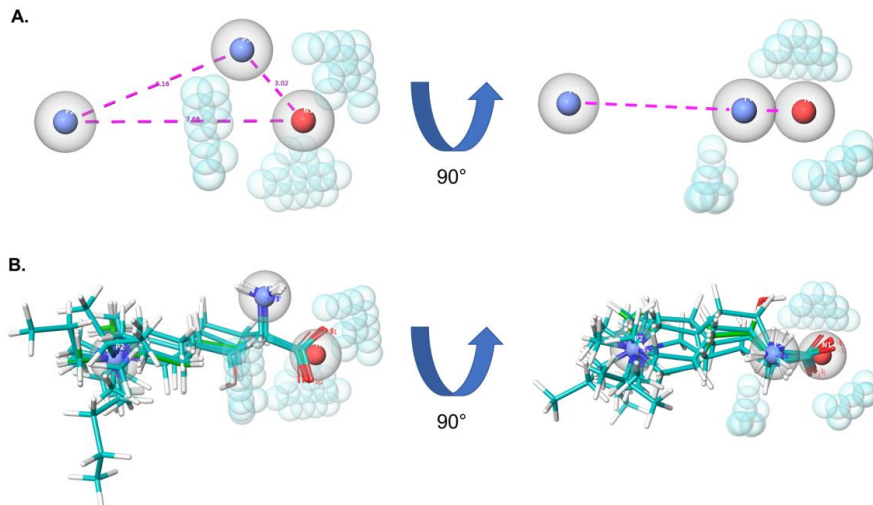


Fig. 2.14. The second pharmacophore model with excluded volumes created from TML and its analogues based on the binding affinities determined by ITC.

A. Pharmacophore model with specified geometric constraints shown from two viewpoints. **B.** Ligand alignment with the pharmacophore model. TML – in green and its analogues (including HTML) – in cyan shown from two viewpoints. Blue spheres – positively charged centres; red sphere – negatively charged centre; light blue spheres – excluded volumes; grey spheres – tolerance radius around the charged centre.

2.5.3. Study of the enzymatic reaction of TMLD

Similarly to BBOX hydroxylating *DL*-carnitine to 3-keto-GBB [29, 37], TMLD also was able to hydroxylate its reaction product, HTML. The possible reaction is shown in Fig. 2.15. Further conversion of 2*S*,3*S*-HTML was observed in the enzymatic reaction with an excess of MBP-TMLD and Fe(II) [≥ 15 and 500 μM , respectively]. The chemical shifts of the newly formed compound at 2.02 (m, 2H), 2.66 (t, 2H), 3.05 (s, 9H), 3.24 (m, 2H), and 3.99 (s, 1H) ppm correspond to the $(\text{CH}_3)_3\text{-N-CH}_2\text{-CH}_2\text{-CH}_2\text{-X-CH}$ fragment, which is likely to be the TML keto product.

On the other hand, it was observed that in the enzymatic reaction with a mixture of 2*S*,3*R*-HTML diastereomers 2*S*,3*R*-HTML reacted more rapidly with the enzyme. The latter is the opposite isomer to the native one (i.e., it did not form from TML in the enzymatic reaction). The binding affinity to the enzyme of the HTML diastereomer mixture (K_D 12.1 \pm 0.1 μM) was determined in the ITC experiments. The K_D was similar to ε -dimethylisopropyl-*L*-lysine (**6**) and ε -dimethylbutyl-*L*-lysine (**7**), however, the binding mechanism was entropy-driven. This is the opposite to TML and resembles the binding mechanisms of compounds **3**, **5**, and **7**.

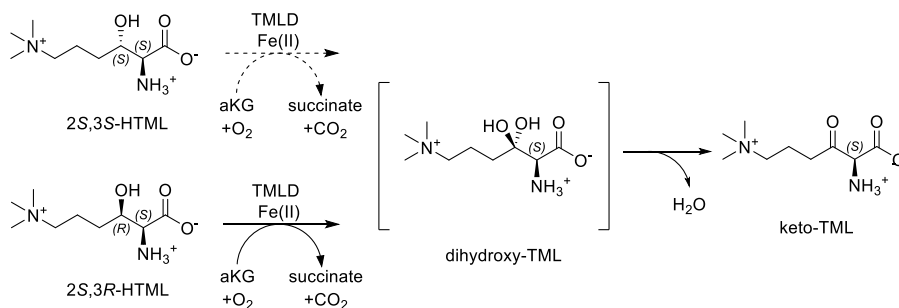


Fig. 2.15. Repeated conversion of HTML by MBP-TMLD enzyme.

2.6. Lipoprotective properties of FABP3 at the cellular level. Establishing a hypothesis

FABP3 is capable of effectively binding TS of various lengths thereby protecting cells from their toxicity. The potential of FABP3 to protect cells from acylcarnitines was tested by titrating PANC-1⁵ cells with palmitoyl carnitine. Fig. 2.16 shows that palmitoyl carnitine is toxic to PANC-1 cells with LC₅₀ being ~ 25 μM . However, the addition of FABP3 increased the cell viability by 20 % on average. Similarly, the cytotoxic effects of palmitoyl carnitine were effectively diminished with overexpression of FABP3 in PANC-1 cells. These data were obtained in collaboration with the Laboratory of Pharmaceutical Pharmacology (LIOS) and were described in the author's publication [38]. Thus, it was hypothesized that FABP3 is capable of binding not only FAs but also FA carnitine esters thereby protecting the cells from their high toxicity. To test this hypothesis, an ITC methodology was developed to examine FAs

⁵ PANC-1 (ATCC® CRL-1469™) pancreatic epithelial carcinoma cells.

and their carnitine esters, as well as protein NMR studies were carried out to characterize the binding mechanism.

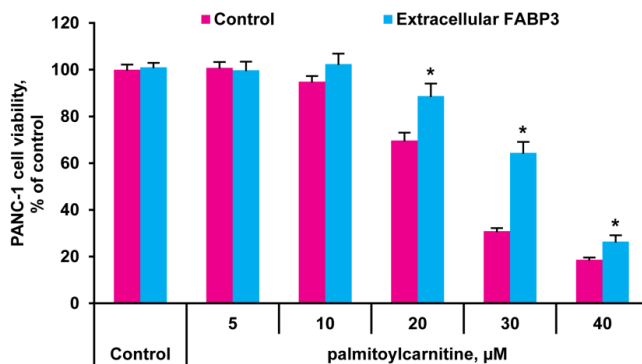


Fig. 2.16. Toxicity of palmitoyl carnitine in the PANC-1 cells after 4 h of incubation in the presence or absence of 60 μM FABP3, respectively, determined by MTT⁶-colourimetric assay.⁷

Reference samples, where only buffer without a protein was added to the cells – in pink. Samples with the recombinant FABP3 additive – in cyan. The first column – control samples, where no palmitoyl carnitine was added. * a significant difference compared to the cells not subjected to FABP3 treatment.

2.7. Experimental conditions search for FABP3 thermodynamic studies

2.7.1. Exploration of additives for solubility and stabilization of FAs solutions

The solubility of FAs in aqueous buffers can be improved by using DMPC⁸/FA liposomes [39], but the heat effects from liposome disruption/reorganization make it difficult to precisely determine the thermodynamic binding parameters. On the other hand, a widely available alternative method where the solubility of FAs is improved by adding bovine serum albumin (BSA) [40] could not be used here due to a very high affinity of BSA towards FAs or their esters that would interfere with the FABP3 experiments. As a result, attempts were made to improve the solubility of FAs in water buffers by adding various supplements such as glycerol, Tween-20, or Triton X-100. The effectiveness of each additive was evaluated by the scattering intensity index of DLS that allowed to estimate the size of particles in the sample. Analysing the DLS data, it was found that the best stabilizing effect was achieved with the addition of 0.1–0.5 % (v/v) Triton X-100, which could stabilize palmitate (C16:0) up to a concentration of 500 μM (scattering intensity $\sim 4537 \pm 149$ kcps⁹). In the case of acylcarnitines,

⁶ MTT – 2,5-diphenyl-2H-tetrazolium bromide. The assay is based on the ability of MTT to change colour from yellow to violet due to the reduction of the tetrazole ring caused by the metabolism of the living cells.

⁷ Data were obtained in collaboration with Laboratory of Pharmaceutical Pharmacology (LIOS). Performed by Kārlis Vilks and Melita Vidēja.

⁸ DMPC – dimyristoylphosphatidylcholine

⁹ kcps – kilo counts per second.

the DLS data showed that the concentration of Triton X-100 did not affect the scattering intensity, but the particle sizes were relatively small in all cases. The scattering intensity for 500 μ M palmitoyl carnitine (C16:0-AC) reached $\sim 3812 \pm 351$ kcps, which is comparable to the scattering intensity of 20 mM potassium phosphate and 50 mM KCl buffer at pH 7.6 (KPi) with 0.50 % (v/v) ethanol additive, 3935 ± 813 kcps.

2.7.2. Effect of additives on FABP3 structure

2D ^1H - ^{15}N HSQC NMR spectra were acquired for ^{15}N -labelled FABP3 by varying the buffer composition in order to examine the effect of additives on its structure. Four spectra were acquired for apo-FABP3: (i) in KPi buffer without additives, (ii) in KPi buffer with 10 % (v/v) glycerol, (iii) in KPi buffer with 0.10 % (v/v) Triton X-100, and (iv) in KPi buffer with 0.25 % (v/v) Triton X-100 additives. The overlay of the spectra obtained is shown in Fig. 2.17 A. As can be seen, all four spectra are in a very good agreement. Minimal changes were observed for ten crosspeaks where one corresponds to the mobile C-terminal residue A133 (hereinafter, FABP3 residue numbering is according to UniProt ID P05413 [21]). The other eight residues (Fig. 2.17 B) belong to the ligand entry portal, while one residue, F71, belongs to the gap region (see Fig. 1.3). All these regions are very mobile, especially in the apo-form of FABP3.

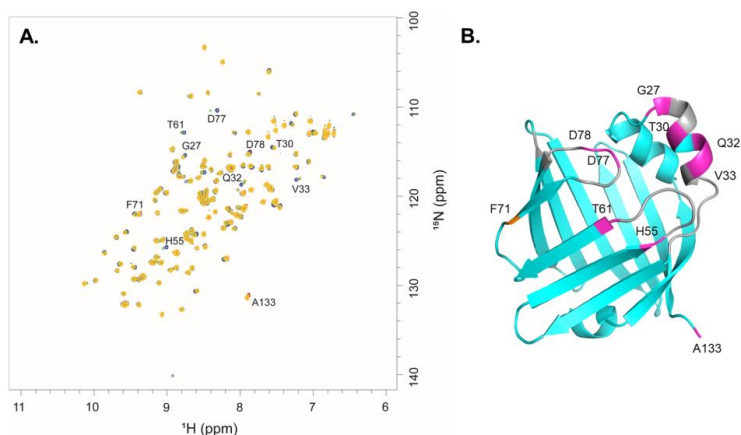


Fig. 2.17. Superposition of 2D ^1H - ^{15}N HSQC spectra of apo-FABP3 upon addition of different buffer additives and mapping of the detected chemical shift perturbations on FABP3 structure (PDB ID 4TKJ).

A. Spectrum in KPi buffer without additives – in blue; with 10 % (v/v) glycerol – in red; with 0.10 % (v/v) and 0.25 % (v/v) Triton X-100 – in green and yellow, respectively. **B.** Chemical shift perturbations mapped on the protein structure in red and orange (ligand entry portal and gap region, respectively); regions in grey – flexible loops that were not assigned at pH 7.6.

Next, the effect of additives on the FABP3-palmitate complex structure was compared. First, the apo-FABP3 spectrum was compared to the spectrum of the FABP3-palmitate complex and the residues with the largest changes in the chemical shifts of their cross peaks were identified (Fig. 2.18 A). A comparison of four FABP3-palmitate spectra acquired by varying

the buffer additives revealed a very high similarity (Fig. 2.18 B). Minimal changes were observed for eight residues, where two belong to the *N*-terminal and *C*-terminal ends, V2 and A133, respectively. The other six residues were the same as those identified in the experiment with apo-FABP3 (Fig. 2.17 A). The obtained data confirm that the used additives neither affect the FABP3 structure nor interfere with FA binding nor alter the conformation of the FABP3-FA complex. The obtained data were described in the author's publication [38].

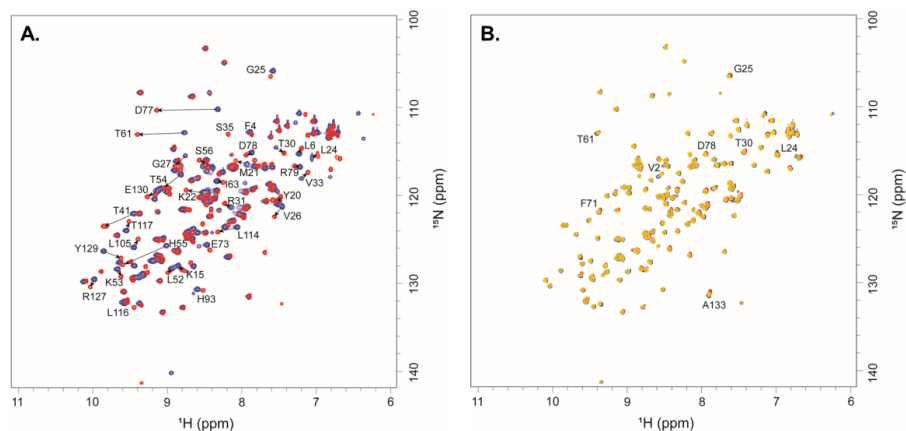


Fig. 2.18. Superposition of 2D ^1H - ^{15}N HSQC spectra of **A.** – apo-FABP3 (in blue) and FABP3-palmitate complex (in red) and **B.** – FABP3-palmitate complex with different buffer additives.

A. Spectra superposition of apo-FABP3 – in blue and FABP3-palmitate (C16:0) – in red in KPi buffer without additives. Black arrows show the shift of the corresponding crosspeak. **B.** Spectra in KPi buffer without additives – in blue; with 10 % (v/v) glycerol – in red; with 0.10 % (v/v) and 0.25 % (v/v) Triton X-100 – in green and yellow, respectively.

2.7.3. Effect of the stabilizing additives on binding thermodynamics parameters

Next, the effect of the above-mentioned stabilizing additives on the binding thermodynamics and affinity of FABP3-FA was evaluated. ITC experiments were performed in KPi buffer with 10 and 20 % (v/v) glycerol and 0.10 and 0.25 % (v/v) Triton X-100 additives, as well as in regular KPi buffer without any additives. Laurate (C12:0) and myristate (C14:0), with CMC = 25.12 and 6.92 mM [41] and solubility – 55 and 20 mg/L H₂O 20 °C [42], were used as the test compounds.

None of the additives affected the stoichiometry of the binding $N \sim 1$ value. However, the binding strength has changed. A comparison of the K_D values of C12:0 for all five titration experiments revealed that the values obtained in KPi buffer and glycerol (regardless of the concentration) are in a good agreement (mean value $0.18 \pm 0.03 \mu\text{M}$). In contrast, K_D weakened ~ 3 and 5.3 -fold, respectively, in samples with 0.10 and 0.25 % (v/v) Triton X-100 additives. In addition, changes in the thermodynamic binding profile were observed. In KPi buffer, both enthalpy and entropy components were negative, i.e., binding-favourable. However, the value of $-T\Delta S$ component was close to zero, and the binding was enthalpy-driven. Glycerol addition

changes the viscosity of the medium. As a result, the bond strength of the non-covalent interactions increased (ΔH increases by absolute value), but $-T\Delta S$ became positive, binding-unfavourable, due to the enthalpy-entropy compensation mechanism [43, 44]. In the case of Triton X-100 additives, similar but much more pronounced changes in the enthalpy and entropy components in comparison to the glycerol additive were observed.

In the case of the longer FAs, e.g., C14:0, the addition of glycerol proved to be ineffective in stabilizing the FA, while the addition of Triton X-100 stabilized the FA well at both 0.10 % and 0.25 % concentrations. However, the affinity of FA for FABP3 in the sample with 0.10 % (v/v) Triton X-100 was twice as strong as in the sample with 0.25 % additive in both cases. Considering the data obtained and the practical implementation of the ITC experiment, 0.10 % (v/v) Triton X-100 was chosen as the optimal concentration of the additive for further titrations.

2.7.4. Determination of binding heat capacity of FABP3-laurate

The change in the heat capacity, ΔC_p , of laurate (C12:0) binding to FABP3 was determined for validation of the ITC assay depending on the buffer composition: in KPi buffer without and with 0.10 % (v/v) Triton X-100 additive. Titration experiments were performed at five different temperatures: 16, 20, 25, 30, and 37 °C. Two linear graphs were constructed from the obtained enthalpy data and ΔC_p values of -0.33 ± 0.01 and -0.22 ± 0.02 kcal·K⁻¹·mol⁻¹ were calculated from linear regression analysis (Fig. 2.19). The difference in the values obtained is minimal and is in a good agreement with that of the phosphate buffer (pK_a 7.198) $\Delta C_p = -0.23$ kcal·K⁻¹·mol⁻¹ [45]. Overall, the trends of the thermodynamic parameters did not change in both buffers, which allows to conclude that the detergent additive did not interfere with FABP3-FA binding and did not affect the binding mechanism. Furthermore, variations of the thermodynamic parameters could be related to the reorganization of the solvation shells and energy changes of the non-covalent interactions.

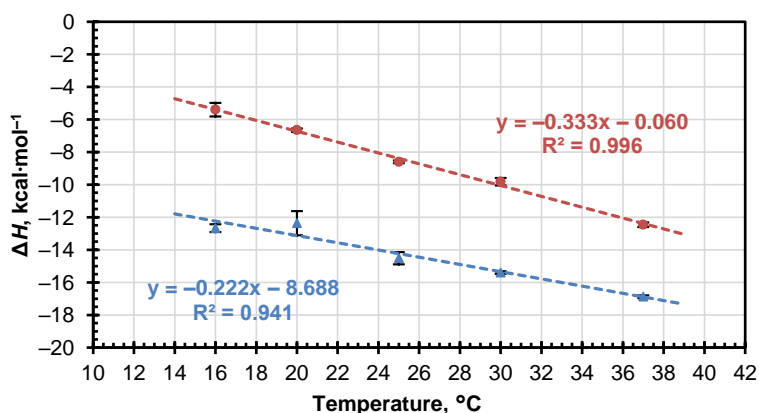


Fig. 2.19. ΔH as a function of temperature determined for FABP3-laurate (C12:0) binding.

KPi buffer (without additives) – trendline in red; KPi buffer with 0.10 % (v/v) Triton X-100 additive – trendline in blue. Points on lines – experimental values of ΔH determined at five different temperatures. The slope of each line represents the heat capacity change, ΔC_p .

2.8. Thermodynamic studies of FABP3

2.8.1. Binding thermodynamics of FABP3-FA

A previously developed and validated ITC assay was applied for the determination of affinities and thermodynamic parameters for the binding of FABP3 with FAs of variable lengths (C8 to C20) and degrees of saturation. In the cases where the solubility of FA allowed (C8–C12), ITC parameters were also determined in the detergent-free buffer. The obtained data are summarized in Table 2.5.

Table 2.5

ITC thermodynamic data of FABP3 interaction with FAs and their esters in KPi buffer at 25 °C

Compound	Short form ¹⁰	0.10 % (v/v) Triton X-100	K_D , μM	ΔG , $\text{kcal}\cdot\text{mol}^{-1}$	ΔH , $\text{kcal}\cdot\text{mol}^{-1}$	$-T\Delta S$, $\text{kcal}\cdot\text{mol}^{-1}$	N ¹¹
caprylate	C8:0	–	1.86 ± 0.05	-7.82 ± 0.02	-8.01 ± 0.09	0.19 ± 0.07	~ 1.0
		+	1.109 ± 0.001	-8.13 ± 0.01	-12.6 ± 0.3	4.5 ± 0.3	~ 1.0
caprate	C10:0	–	0.252 ± 0.004	-9.01 ± 0.01	11.09 ± 0.08	2.08 ± 0.08	~ 1.0
		+	0.56 ± 0.02	-8.535 ± 0.007	-13.2 ± 0.3	4.7 ± 0.3	~ 1.0
laurate	C12:0	–	0.20 ± 0.02	-9.12 ± 0.06	-8.60 ± 0.08	-0.53 ± 0.02	~ 1.0
		+	0.57 ± 0.06	-8.54 ± 0.06	-14.5 ± 0.4	6.0 ± 0.3	~ 1.0
myristate	C14:0	+	0.3 ± 0.1	-8.9 ± 0.2	-10.9 ± 0.4	1.9 ± 0.2	~ 1.0
palmitate	C16:0	+	0.14 ± 0.02	-9.34 ± 0.07	-8.7 ± 0.9	-0.6 ± 0.8	~ 1.0
stearate	C18:0	+	0.7 ± 0.1	-8.34 ± 0.04	-6.4 ± 0.4	-2.0 ± 0.4	~ 1.0
oleate	C18:1 <i>cis</i> - Δ^9	+	0.29 ± 0.03	-8.93 ± 0.06	-10.0 ± 0.4	1.1 ± 0.5	~ 1.0
elaidate	C18:1 <i>trans</i> - Δ^9	+	0.21 ± 0.02	-9.12 ± 0.06	-8.0 ± 0.9	-1.1 ± 0.9	~ 1.0
eicosapentaenoate (EPA)	20:5 <i>cis</i> - $\Delta^{5,8,11,14,17}$	+	1.6 ± 0.2	-7.90 ± 0.07	-17.4 ± 0.7	9.5 ± 0.8	~ 1.0
palmitoyl-CoA	C16:0-CoA	–	8.9 ± 1.2	-6.90 ± 0.08	-5.04 ± 0.09	-1.86 ± 0.01	~ 1.0
EPA-carnitine	20:5 <i>cis</i> - $\Delta^{5,8,11,14,17}$ -AC	–	14.83 ± 0.08	-6.61 ± 0.03	-2.43 ± 0.09	-4.19 ± 0.06	~ 1.0
myristoyl carnitine	C14:0-AC	–	11.3	-6.7	-1.1	-5.7	~ 0.5
oleoyl carnitine	C18:1 <i>cis</i> - Δ^9 -AC	–	2.21 ± 0.07	-7.72 ± 0.01	-4.6 ± 0.2	-3.1 ± 0.2	~ 0.5
elaidoyl carnitine	C18:1 <i>trans</i> - Δ^9 -AC	–	2.19 ± 0.04	-7.72 ± 0.02	-4.29 ± 0.06	-3.43 ± 0.08	~ 0.5

¹⁰ Number of carbons: number of unsaturated bonds and their positions.

¹¹ In the ITC experiment, the stoichiometry, N , shows either protein-ligand binding ratio or the amount of the active protein in the sample. Here, N is assessed assuming that protein is 100 % active and completely delipidated.

C8:0 was found to be the weakest while C16:0 – the strongest FABP3 binder. C18:0 and C14:0 were bound at least 2-fold weaker in comparison to C16:0. All tested FAs had the same enthalpy-driven binding mechanism with dominating ΔH component. Several medium-chain and long-chain FAs (C8:0–C14:0) had the entropy component binding-unfavourable, close to zero (C16:0), or binding-favourable (C18:0). Both monounsaturated FAs (C18:1) gave highly similar binding affinities and thermodynamic parameters indicating that *cis/trans* double bond configuration did not affect FA binding in the binding site of FABP3. Moreover, polyunsaturated FA, EPA, showed a relatively weak binding that was similar to C8:0. In comparison to C8:0, EPA had an improvement in ΔH by $\sim 9.4 \text{ kcal}\cdot\text{mol}^{-1}$ and a decrease in $-T\Delta S$ by a similar value. Assuming that the flexibility of EPA is restricted by five *cis* double bonds, it most probably adopts a bent conformation in the binding site of FABP3 causing reorganization of the binding site due to steric hindrance, as indicated by an increase in the value of $-T\Delta S$. On the other hand, the restricted flexibility positively affected the protein-ligand non-covalent interactions. The obtained data were described in the author's publication [38].

2.8.2. Binding thermodynamics of FABP3-acylcarnitines and palmitoyl-CoA

Continuing thermodynamic studies, attempts were made to determine the binding parameters for FA carnitine and CoA esters. Interestingly, Triton X-100 completely blocked ester binding even at a concentration of 0.10 % (v/v) while in the case of FAs, the detergent additive did not interfere with binding. The results obtained indicate that esters likely have a different recognition mechanism than FAs. Furthermore, the binding was only observed for well-soluble compounds – EPA-carnitine, palmitoyl-CoA, and monounsaturated C18:1-*cis/trans*- Δ^9 -carnitines when the reaction was carried out in KPi buffer without additives (Table 2.5). In comparison to the corresponding FAs, the ΔH value (in the absolute values) decreased by a factor of two indicating a weakening of non-covalent interactions that was partially compensated by a binding-favourable $-T\Delta S$, which is 3-fold larger than that of the corresponding monounsaturated FAs. All four esters were bound to FABP3 with a relatively similar thermodynamic profile. However, a decrease in binding stoichiometry, N , from 1.0 to 0.5 was observed for C18:1-*cis/trans*- Δ^9 -carnitines. This was unexpected, as such stoichiometry suggests that one ligand molecule simultaneously binds to two protein molecules. Changes in the protein-ligand concentrations and their ratios did not affect this result. These data indicate that a novel binding mechanism for monounsaturated acylcarnitines was observed. The obtained data were described in the author's publication [38].

2.8.3. Studies of saturated FA carnitine esters

Considering that mono- and polyunsaturated FA carnitine esters successfully bind to FABP3, it was expected that saturated FA carnitine esters of similar lengths should also bind to FABP3, however, experiments with them were less successful. Despite better solubility in aqueous buffers (especially at low pH) in comparison to FAs, in the case of longer acylcarnitines, micellization was observed [46, 47] that hinders their binding to FABP3. This

effect is especially pronounced for palmitoyl carnitine which has a CMC of 15 μM only [47]. The only saturated FA carnitine ester that was able to bind in the ITC experiment in KPi buffer (without additives) was C14:0-AC which bound as weakly as EPA-AC and with similar thermodynamic parameters, but with a stoichiometry of ~ 0.5 (see Table 2.5). It demonstrates that the carnitine esters of saturated and monounsaturated FAs should bind to FABP3 by a similar mechanism.

In order to improve the solubility of palmitoyl carnitine, DMPC/acylcarnitine liposomes were prepared following the protocol from Matsuoka *S. et. al* [39]. As a control, DMPC/laurate and DMPC/myristate liposomes were also prepared. Unfortunately, it was not possible to detect binding heat effects in the ITC experiment by utilizing this method for the determination of thermodynamic parameters for C12:0-AC, C14:0-AC, and C16:0-AC esters. On the other hand, two samples (C12:0-AC and C14:0-AC) showed minimal changes, while no changes in the chemical shifts were observed in the spectrum of C16:0-AC in the NMR experiments.

2.9. Effect of palmitoyl carnitine on FABP3 at low pH

Acylcarnitines are highly soluble and do not form micelles at low pH. Thus, FABP3-palmitoyl carnitine binding studies were performed at non-physiological pH: 5.4 and 3.6. 2D ^1H - ^{15}N HSQC spectra were used to confirm that apo-FABP3 retains its structure in both buffers under non-physiological pH. Next, the ability of palmitate (C16:0) and palmitoyl carnitine (C16:0-AC) to bind to FABP3 in different pH environments was tested. In the case of palmitate, the protein-ligand binding was observed at pH 7.6 and 5.4. Moreover, the changes in the chemical shifts observed in the spectra had similar trends. On the other hand, palmitate did not bind to FABP3 at pH 3.6. Most probably, it is related to the changes in the protonation states of the residues in the vicinity to the ligand entry portal and protonation of the palmitate carboxyl group (pK_a 4.75). This prevents the formation of electrostatic interactions that drive the ligand into the binding site [27]. In the case of palmitoyl carnitine, changes in the spectrum at pH 7.6 are much more pronounced than at pH 5.4, however, they are still very small to unambiguously identify the complex formation. On the other hand, the disappearance of protein signals was observed in the spectrum at pH 3.6, no precipitation was formed in the sample as well. It seems that macromolecular complexes were formed in the sample whose relaxation was too fast on the NMR time scale. Thus, the signal loss was observed. To test this hypothesis, NMR samples in acetate buffer were investigated by DLS.

DLS data showed that the particle size of apo-FABP3 (Fig. 2.20 A) in the acetate buffer at pH 3.6 was ~ 56 d.nm (95.8 %) and the sample was very homogeneous. The resulting size corresponds with the hydrodynamic radius of the protein. The palmitoyl carnitine sample (Fig. 2.20 B) was also very homogeneous at low pH. Here, all particles were ~ 7.3 d.nm in size (99.7 %). On the other hand, the distribution in the particle size of ~ 80.5 d.nm (50 %) and ~ 8.6 d.nm (50 %) was observed in the FABP3-palmitoyl carnitine sample (Fig. 2.20 C). Overall, this indicates that a palmitoyl carnitine layer was formed on the protein. Specifically, two C16:0-AC particles were attached to one FABP3 particle ($56 + 8.6 + 8.6 = 73.2 \approx 80$ d.nm). Furthermore, it can be seen that only one-half of the added palmitoyl carnitine was bound to

the protein according to this distribution. Particles of two sizes ~ 54 d.nm (56 %) and 1462 d.nm (48 %) were also observed in the sample with FABP3-palmitate (Fig. 2.20 D). This also explains why C16:0 did not bind to FABP3, as all ligand molecules formed irregular macromolecular aggregates. On the other hand, the protein particles remained unchanged and match the sizes of apo-FABP3 particles.

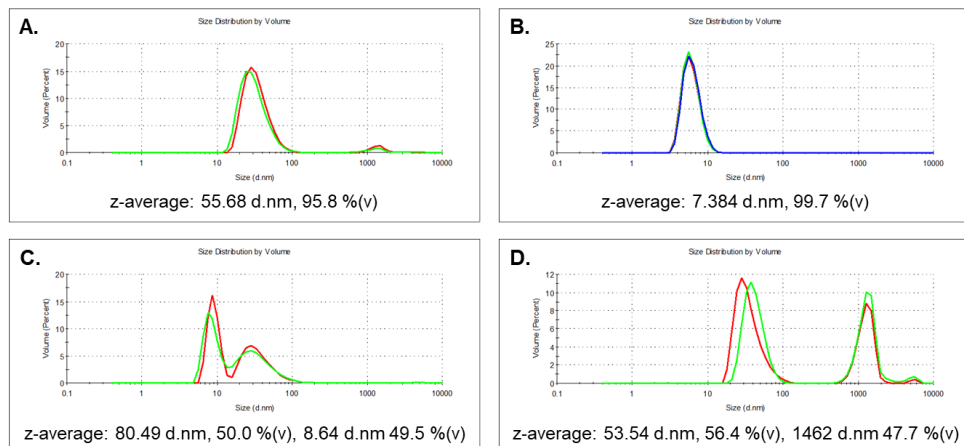


Fig. 2.20. DLS measurements **A.** apo-FABP3, **B.** palmitoyl carnitine, **C.** complex of FABP3-palmitoyl carnitine, and **D.** complex of FABP3-palmitate in acetate buffer at pH 3.6.

2.10. Validation of binding to FABP3 by NMR

2.10.1. Basic principles of chemical shift perturbation analysis

Chemical shift perturbation (CSP) analysis was performed in order to evaluate and quantify the changes detected in the NMR spectra. It is based on the high sensitivity of 2D ^1H - ^{15}N HSQC spectrum to any changes in the sample. The crosspeak shifts observed in the spectra were calculated using the assigned apo-FABP3 and FABP3-complex spectra and Equation (1) with a scaling factor, $\alpha = 0.10$ [48, 49]. Afterwards, these shifts were visualized as a histogram or shown graphically by assigning CSP values in the form of a colour gradient that changes from dark blue to red. This colouring is applied to the 3D structure of the protein, thus providing an opportunity for a better understanding of the reasons and nature of the defined changes, as well as evaluating the differences between binding of various ligands to the protein.

$$\Delta\delta = \sqrt{\frac{1}{2}[\delta_H^2 + (\alpha \cdot \delta_N)^2]}, \quad (1)$$

where

- $\Delta\delta$ – CSP;
- δ_H – proton chemical shifts, ppm;
- δ_N – nitrogen chemical shifts, ppm;
- α – scaling factor (0.10–0.45).

2.10.2. CSP Analysis of FABP3-ligand complexes

The previously described CSP analysis method was applied to all FABP3-ligand complexes studied in this work. In total, 17 compounds were analysed where 9 ligands were FAs and 8 – were FA esters. As can be seen from the obtained data, the binding of FAs (Fig. 2.21 A) causes more changes in the protein conformation than the binding of FA ester (Fig. 2.21 B). Moreover, as the FA length increases, larger perturbations were observed in the β_A – β_J strands of the β -barrel (see Fig. 1.3) in the depth of the binding site. In all cases, except for C8:0-AC and C16:0-AC, significant changes were observed in the α_{II} helix region which is closer to the ligand entry portal as well. Unfortunately, the loops forming the entry portal were not assigned at pH 7.6 (grey regions), but the changes experienced by their adjacent residues potentially indicate large conformational changes in this region.

The following 20 residues were identified by analysing positions with the largest changes (CSP ≥ 0.2 ppm): K10, L11, Y20*, V26, G27, T30*, Q32, V33, A34*, T41, T54, H55, S56*, T61, D77, L105*, L114, L116*, R127, and Y129 (Fig. 2.21 A). Here, residues marked with * were observed for all FAs, except for the shortest one, C8:0. In the case of FA esters, less or no CSPs were observed on the β_A – β_D strands. Furthermore, a comparison of the changes observed reveals that changes in the FABP3 structure caused by C14:0-AC, C18:0-1-*cis/trans*- Δ^9 -AC, and EPA-AC resemble binding of C8:0. In addition, more changes were observed in the β_I – β_J strands. Overall, the following residues showed a significant CSP effect for acylcarnitines: W9, K10, V12, D18, Y20, K22, G27, Q32, V33, A34, T54, H55, L92, T117, T119, T128, Y129, and E130 (Fig. 2.21 B).

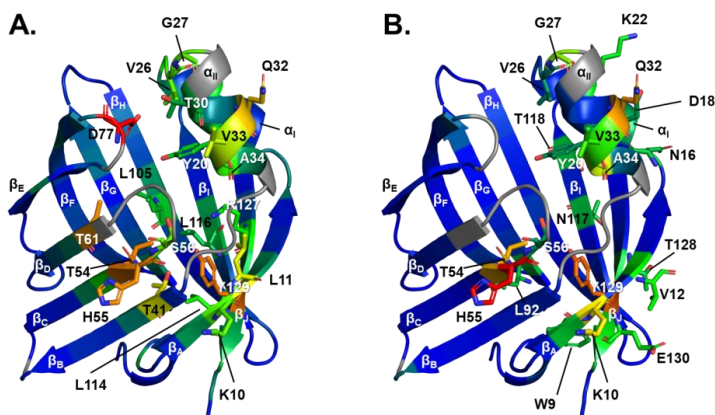


Fig. 2.21. Mapping of the CSPs on FABP3 structure (PDB ID 3WVM) caused by binding of **A.** elaidate (C18:1-*trans*- Δ^9) and **B.** elaidoyl carnitine (C18:1-*trans*- Δ^9 -AC) with assigned residues that participate in ligand recognition. Prepared using PyMOL software [20].

Thus, it can be concluded that acylcarnitines and palmitoyl-CoA bind to FABP3 only on one side of the β -barrel and most likely do not form a U-shaped conformation. R127, which usually forms a salt bridge with the negatively charged carboxyl group, does not show CSP for acylcarnitines. Most probably, this occurs as the ligand is in the ester form now and *L*-carnitine

cannot enter the hydrophobic binding site and make contact with its carboxyl group. The obtained data were described in the author's publication [38].

2.10.3. Modelling of FABP3-acylcarnitine complexes by IFD calculations

The IFD method was used to model FABP3-acylcarnitine complexes generating 200 ligand conformations. The precise binding conformation of acylcarnitines is unknown, thus, it is impossible to determine the number of water molecules in the binding site. For this purpose, several protein models that differed only by the amount of water molecules were created *in silico*. Five complexes of FABP3 (PDB ID 4TKJ) with 30, 24, 12, 2, and 0 water molecules were further used in IFD SP molecular docking [50, 51]. The best results were achieved using the structures with 0–12 water molecules, which minimally restrict the volume of the binding site and do not alter its hydrophilicity. As a result, binding of hydrophobic FA esters was observed.

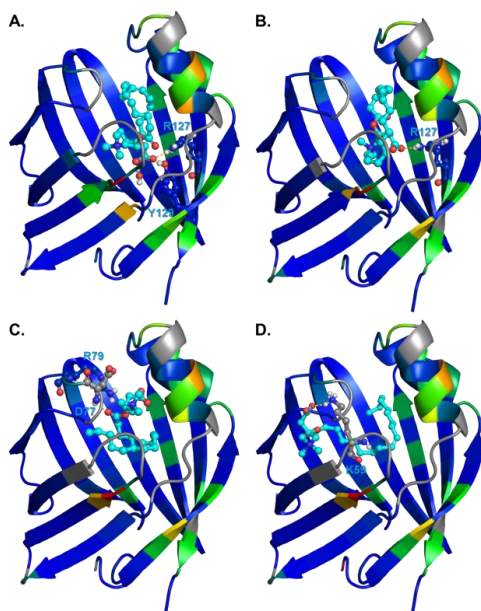


Fig. 2.22. Complexes of FABP3-Acylcarnitine Modelled by IFD.

A. FABP3-oleoyl carnitine (C18:1-*cis*- Δ^9 -AC) in a conformation similar to FA. **B.** FABP3-EPA-AC in a conformation similar to FA. **C.** FABP3-oleoyl carnitine in an inverted conformation. **D.** FABP3-oleoyl carnitine in an open conformation. Protein is coloured according to the CSPs and shown as ribbons. Ligand is shown in cyan as balls-and-sticks. Residues that participate in hydrogen bond formation with a ligand are shown as balls-and-sticks (colouring by CSPs). Hydrogen bonds are shown as yellow dashed lines. Prepared using PyMOL software [20].

In the majority of the complexes, IFD placed acylcarnitines in the conformations that mimic the U-shaped conformation of the long-chain FAs (Fig. 2.22 A, B) and induced the formation of contacts with R127 and Y129. In the second conformation, *L*-carnitine moiety is positioned directly at the entrance of the ligand entry portal (Fig. 2.22 C) and it formed a hydrogen bond

with D77, as well as a salt bridge with R79. Meanwhile, the end of the lipophilic alkyl chain is placed directly in the gap between the β_D and β_E strands. The third conformation is one of the most interesting. Here, *L*-carnitine moiety is directed outward through the gap region between β_D – β_E strands and forms a hydrogen bond with K59 (Fig. 2.22 D). The entire lipophilic part of the ligand remains inside the β -barrel, closer to the β_I – β_J strands, as expected by CSP experimental data as well.

FA-like conformations seem to be doubtful, as the experimental CSP data did not confirm the formation of contacts with R127 and Y129. The analysis of the obtained conformations reveals that IFD overestimates the formation of the electrostatic contacts, as in most complexes carboxyl group of *L*-carnitine was bound to one of the positively charged residues in the FABP3 binding site, which contradicts NMR experiments. On the other hand, reverse and open binding conformations (Fig. 2.22 C, D) that are in significantly better agreement with the experimental data were observed in a small number of complexes.

2.11. Studies on binding mechanism of monounsaturated acylcarnitines

ITC experiments revealed that monounsaturated acylcarnitines were bound to FABP3 by a different mechanism as the stoichiometry, N , was reduced to ~ 0.5 (see Fig. 2.23 A). One possible explanation could be that one ligand molecule is bound by two protein molecules. In order to better characterize the binding mechanism, ITC and NMR competitive binding experiments were performed, where the ability of monounsaturated acylcarnitines to substitute FAs in the binding site of FABP3 was evaluated.

Firstly, ITC experiments were performed. The competition was performed with three FAs of variable length that are soluble in an aqueous buffer without any additional supplements. The obtained data were summarized in Fig. 2.23. In the first experiment, FABP3 was saturated with C8:0 and afterwards titrated with elaidoyl carnitine (C18:1-*trans*- Δ^9 -AC) (Fig. 2.23 B). Here, C18:1-*trans*- Δ^9 -AC substituted C8:0 in the binding site of FABP3 maintaining the same binding mechanism with $N \approx 0.5$ as well. In the next experiment (Fig. 2.23 C), FABP3 was first saturated with C10:0 and then titrated with elaidoyl carnitine. No binding heat effects were observed in this experiment.

In the opposite experiment, the protein was saturated with C18:1-*trans*- Δ^9 -AC and then titrated with C10:0 (Fig. 2.23 D). Here, binding of FA to the protein was detected, but unexpectedly, $N \approx 0.5$ was obtained. Such an experiment is only possible if C10:0 displaced elaidoyl carnitine from one binding site and did not compete for the second one. This observation suggests that one of the binding sites for monounsaturated acylcarnitines is in the binding site of FABP3 and C10:0 is unable to compete for it due to weak affinity. On the other hand, the second binding site is either not associated with the binding cavity or the binding occurs in a different conformation that has a weaker affinity. In the final titration of this experimental series, FABP3-C18:1-*trans*- Δ^9 -AC complex was titrated with C12:0 (Fig. 2.23 E). Here, the binding of FA to FABP3 and displacement of elaidoyl carnitine was also observed, but in contrast with C10:0, stoichiometry returned to ~ 1.0 . This means that, unlike C10:0, C12:0 can substitute monounsaturated acylcarnitines from both of their binding sites.

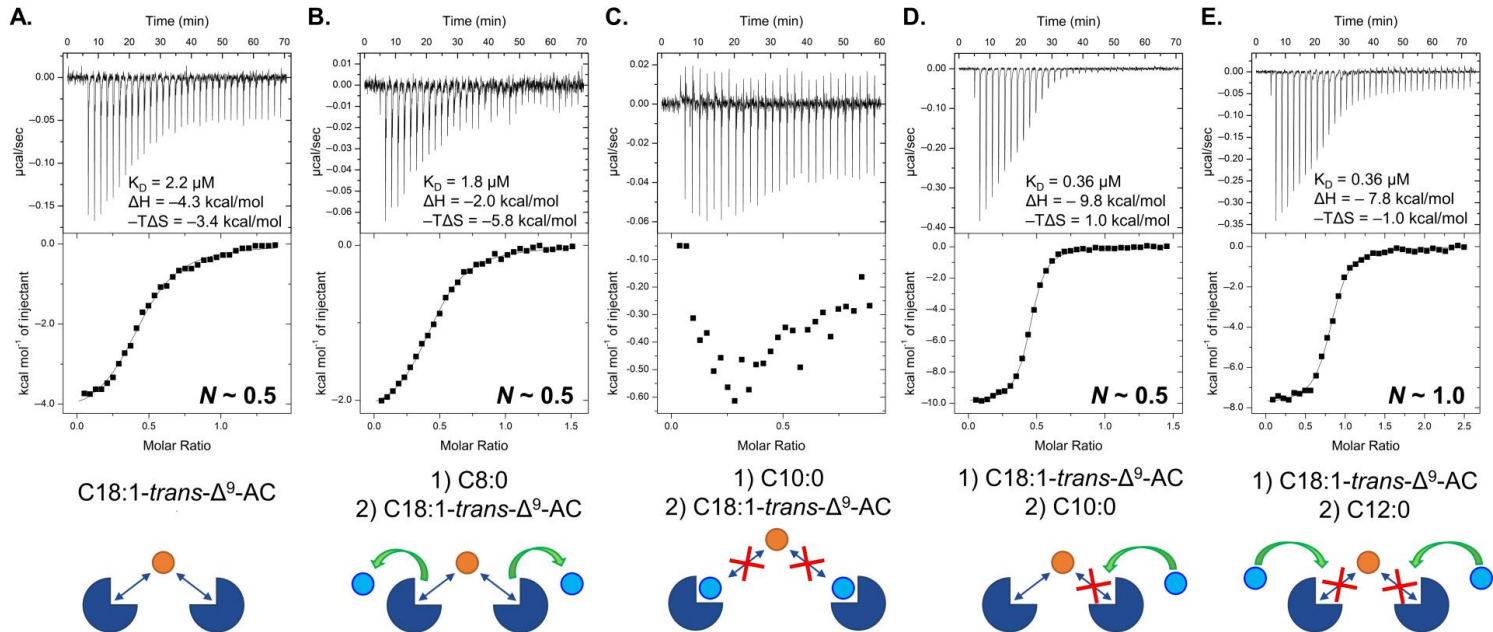


Fig. 2.23. Competitive binding studies of FABP3 between elaidoyl carnitine (C18:1-*trans*- Δ^9 -AC) and three FAs of different chain length in KP1 buffer at 25 °C (top) and schematic representation of the ligand binding and competition (bottom).

- A.** Reference titration of elaidoyl carnitine to apo-FABP3 solution. Schematically protein is shown as the dark blue sector but acylcarnitine – as orange circle. **B.** FABP3-C8:0 complex titrated with elaidoyl carnitine. Schematically FAs are shown as cyan circles. **C.** FABP3-C10:0 complex titrated elaidoyl carnitine. No competition was observed. **D.** FABP3-elaidoyl carnitine complex titrated with C10:0. Schematics show that FA (cyan circle) replaced acylcarnitine (orange circle) from only one of its binding sites. **E.** FABP3-elaidoyl carnitine complex titrated with C12:0. Schematics show that FA (cyan circle) replaced acylcarnitine (orange circle) from both of its binding sites. Green arrows point to the successful competition event between ligands.

To elucidate how monounsaturated acylcarnitines compete with FAs for the binding site of FABP3, additional protein NMR experiments were performed using similar approach as in the ITC experiments. Firstly, the protein was saturated with the first ligand and a 2D ^1H - ^{15}N HSQC spectrum was acquired. Afterwards, the second ligand was added to the NMR tube and the spectrum was acquired once again. Fig. 2.24 shows assigned crosspeaks with the largest CSPs that should be analysed when examining the three-component mixture as a reference. The largest difference between the two spectra occurred due to the disappearance of some of the crosspeaks in the second spectrum (Fig. 2.24 B, marked with *). Thus, the disappearance of the crosspeaks G27, R31, V33, S35, T61, and D77 should be considered during the analysis of the competition experiment spectra between C8:0 and elaidoyl carnitine (Fig. 2.25 A). On the other hand, some signals returned to their initial positions while others disappeared when elaidoyl carnitine displaced FA from the FABP3 binding site. The spectra were in a good agreement with each other confirming the binding of elaidoyl carnitine which substituted C8:0. Next, two opposite experiments were performed between the FABP3-elaidoyl carnitine complex and C10:0 and C12:0 FAs as the competitive ligands. The results are shown in Fig. 2.25 B and C, respectively. Here, the analysis was simplified as the binding of elaidoyl carnitine resulted in the disappearance of some of the signals from the spectrum. On the other hand, new crosspeaks were observed after the displacement of acylcarnitine from the binding site of FABP3 by the stronger binder, FA. These data showed that both C10:0 and C12:0 were bound to the FABP3 binding site producing the same changes as in FABP3-FA complexes.

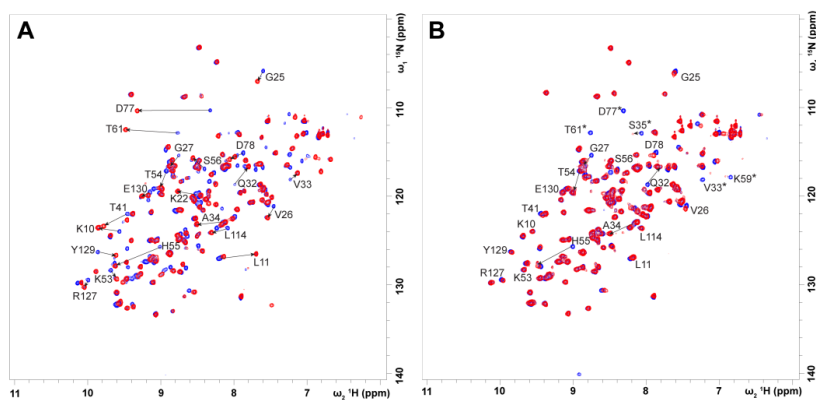


Fig. 2.24. Superposition of 2D ^1H - ^{15}N HSQC spectra with assigned residues: **A.** FABP3-C8:0 and **B.** FABP3-C18:1-*trans*- Δ^9 -AC complexes in KPi buffer at pH 7.6.

Superposition of the spectra: apo-FABP3 – in blue and FABP3-C8:0 (A) or FABP3-C18:1-*trans*- Δ^9 -AC complex (B) – in red with assigned residues that showed significant CSPs. Black arrows show the shift of the corresponding crosspeak. * marks the crosspeaks that have disappeared upon binding of the acylcarnitines.

Thus, it can be seen that monounsaturated acylcarnitines bind to the binding site of FABP3; however, they cannot adopt the same conformation as FAs due to their structure. Currently, it is not fully understood how one ligand binds with two protein molecules. Possibly, binding occurs through the carnitine moiety, but carnitine alone did not bind to FABP3 (no binding was observed in either ITC or NMR experiments). However, it is possible that binding occurs only

for carnitine esters with the length of FA “tail” \geq C14 that acts as an “anchor” and fixes acylcarnitine inside FABP3. The obtained data were described in the author’s publication [38].

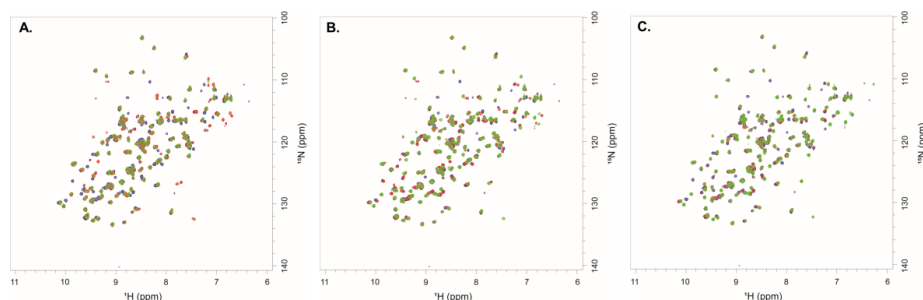


Fig. 2.25. Superposition of 2D ^1H - ^{15}N HSQC spectra of the competitive binding experiments of FABP3 complexes in KPi buffer at pH 7.6.

A. FABP3 in complex with C8:0 with added elaidoyl carnitine (C18:1-*trans*- Δ^9 -AC). **B.** FABP3 in complex with C18:1-*trans*- Δ^9 -AC with added C10:0. **C.** FABP3 in complex with C18:1-*trans*- Δ^9 -AC with added C12:0. Apo-FABP3 – in blue; complex with the first ligand – in red; and complex with the second ligand – in green.

2.12. Expanding the substrate scope of FABP3

To sum up, the experimental data of FABP3, FA, and acylcarnitine binding reveal that FABP3 is potent to bind not only FAs of different lengths but also acylcarnitines of medium and long-chain lengths (Table 2.6). The physicochemical methods applied allowed to determine that mono- and polyunsaturated acylcarnitines bind to FABP3 with high reliability, but with the affinity of one order of magnitude lower than that of the corresponding long-chain FAs.

Table 2.6

Summary of FABP3-ligand binding studies

Compound	Short form	Binding in ITC	Binding in NMR	New binding mechanism
caprylate	C8:0	+	+	–
caprate	C10:0	+	+	–
laurate	C12:0	+	+	–
myristate	C14:0	+	+	–
palmitate	C16:0	+	+	–
stearate	C18:0	+	+	–
oleate	C18:1 <i>cis</i> - Δ^9	+	+	–
elaidate	C18:1 <i>trans</i> - Δ^9	+	+	–
EPA	20:5 <i>cis</i> - $\Delta^{5,8,11,14,17}$	+	+	–
palmitoyl-CoA	C16:0-CoA	+	+	–
capryloyl carnitine	C8:0-AC	no binding	no binding	–
lauroyl carnitine	C12:0-AC	no binding	+	–
myristoyl carnitine	C14:0-AC	+	+	+
palmitoyl carnitine	C16:0-AC	cannot be measured	only at low pH	no data
oleoyl carnitine	C18:1 <i>cis</i> - Δ^9 -AC	+	+	+
elaidoyl carnitine	C18:1 <i>trans</i> - Δ^9 -AC	+	+	+
EPA-carnitine	20:5 <i>cis</i> - $\Delta^{5,8,11,14,17}$ -AC	+	+	–

Positive significant effect indicating undoubtful binding event – in green. Binding effects were weak – in yellow. No binding was observed, or the compound was insoluble under specified experimental conditions – in white.

MAIN RESULTS OF THE THESIS

1. An effective mimetic of TMLD that is potent to hydroxylate TML or its analogues cannot be produced by introducing 2 or 4 mutations in the active site of BBOX. However, binding between BBOX mutants and TML is observed but it did not result in the catalytic reaction.
2. The model of TMLD generated by artificial intelligence (AlphaFold) is found to be more stable than similar models generated by homology modelling programs. Defined by RMSD, RMSF, and statistical analysis of MD simulations.
3. AlphaFold reproduces the active site of TMLD with relatively high accuracy as indicated by pLDDT score and expected position error analysis. Modelling results are in a good agreement with the experimental data.
4. The stability and activity of the recombinant TMLD can be significantly improved by the reduction of the expression temperature and purification in the presence of a high concentration of sugar supplements.
5. Co(II) and Zn(II) cations can be used as Fe(II) isosteres in the active site of TMLD. However, Ni(II) that gave better results in the case of BBOX binding experiments did not work as Fe(II) isostere in the case of TMLD.
6. A novel methodology for the characterization of potential TMLD inhibitors by ITC was developed.
7. The correlation between substrate conversion by TMLD, succinate/hydroxylated product ratio, and the binding mechanism was found.
8. The pharmacophore model for TMLD substrate analogues was developed based on the ITC data.
9. TMLD as well as BBOX is potent to hydroxylate 2*S*,3*S*-HTML and 2*S*,3*R*-HTML to keto-TML. However, the hydroxylation of the native reaction product, 2*S*,3*S*-HTML, is significantly slower and unfavourable in comparison to the conversion of 2*S*,3*R*-HTML.
10. The ITC methodology for the saturated and unsaturated FAs of variable length in the presence of a solubility-enhancing detergent additive, Triton X-100, was developed and validated. Thus, its application allowed to determine parameters of binding thermodynamics and evaluate binding affinity.
11. The substrate scope of FABP3 was expanded. FABP3 is able to bind both FA and carnitine or CoA esters. A new binding mechanism was observed in the case of monounsaturated acylcarnitine interaction with FABP3.
12. The affinity of long-chain acylcarnitines and CoA esters to FABP3 is by at least one order of magnitude lower than that for the corresponding FA. *L*-Carnitine and CoA prevent acylcarnitines from entering deeply inside the binding site of FABP3, thus, forming the protein-ligand conformation with suboptimal contact network and binding unfavourable solvation or conformational rearrangements.
13. Backbone assignments of apo-FABP3 and 14 FABP3-ligand complexes were performed. Chemical shifts were used in extensive CSP analysis. Possible binding conformations of acylcarnitines were generated based on CSP data and *in silico* molecular docking.
14. Competition between acylcarnitines and FA for the binding pocket of FABP3 was proven.

CONCLUSIONS

1. Newly developed ITC assay allowed to characterize binding of substrate-like compounds to TMLD. In combination with the enzymatic assay data, it allowed to determine both thermodynamic parameters (binding affinity, enthalpy, and entropy) and ligand potential to serve as a substrate.
2. Two different binding mechanisms were discovered, enthalpy- and entropy-driven, that differ by ligand-caused changes in the active site of TMLD. A correlation between TMLD substrate conversion and binding mechanism was found. Substrates that bind to the TMLD by entropy-driven binding mechanisms were hydroxylated to a lesser extent.
3. Uncoupling between α KG turnover and hydroxylation reaction of several TML analogues was observed. Hence, such compounds occupy the active site of TMLD for a longer period without production of the reaction product. Thus, these compounds can be used for the *de novo* design of TMLD inhibitors due to prolonged residence times.
4. The TMLD pharmacophore model developed confirms the necessity of the three functional elements for successful substrate binding. It can be used to predict binding affinities towards TMLD for new TML analogues.
5. FABP3 is potent to bind both saturated and unsaturated fatty acids as well as corresponding long-chain acylcarnitines or CoA esters [as determined by physical chemistry methods (ITC and NMR)]. Polyunsaturated acylcarnitines and CoA esters bind to FABP3 active site in the same way as fatty acids, while long-chain monounsaturated acylcarnitines bind by a different mechanism where one ligand molecule is potent to bind two protein molecules.
6. Acylcarnitines displace short fatty acids (including caprylate, C6:0) from the active site of FABP3. Caprate (C10:0) competes with acylcarnitines only for the second less potent binding site of FABP3, while laurate (C12:0) completely replaces acylcarnitines from their both binding sites.
7. The experimental data obtained suggest that FABP3 is potent to bind acylcarnitines and protect cells from their damage and acute toxicity, thus, acting similarly to a cardio-protective medicine. This suggests one of the possible therapies by initiation of the FABP3 overexpression in the target tissues (i.e., heart muscle) using mRNA vaccine approach.

REFERENCES

- [1] World Health Organization. Global Health Estimates: Life expectancy and leading causes of death and disability. https://www.who.int/healthinfo/global_burden_disease/estimates/en/index1.html.
- [2] Dambrova, M.; Zuurbier, C. J.; Borutaite, V.; Liepinsh, E.; Makrecka-Kuka, M. Energy Substrate Metabolism and Mitochondrial Oxidative Stress in Cardiac Ischemia/Reperfusion Injury. *Free Radic. Biol. Med.* **2021**, *165*, 24–37.
- [3] Liepinsh, E.; Makrecka-Kuka, M.; Volska, K.; Kuka, J.; Makarova, E.; Antone, U.; Sevostjanovs, E.; Vilskersts, R.; Strods, A.; Tars, K.; Dambrova, M. Long-Chain Acylcarnitines Determine Ischaemia/Reperfusion-Induced Damage in Heart Mitochondria. *Biochem. J.* **2016**, *473* (9), 1191–1202.
- [4] Dambrova, M.; Makrecka-Kuka, M.; Kuka, J.; Vilskersts, R.; Nordberg, D.; Attwood, M. M.; Smesny, S.; Sen, Z. D.; Guo, A. C.; Oler, E.; Tian, S.; Zheng, J.; Wishart, D. S.; Liepinsh, E.; Schiöth, H. B. Acylcarnitines: Nomenclature, Biomarkers, Therapeutic Potential, Drug Targets, and Clinical Trials. *Pharmacol. Rev.* **2022**, *74* (3), 506–551.
- [5] Liepinsh, E.; Kuka, J.; Vilks, K.; Svalbe, B.; Stelfa, G.; Vilskersts, R.; Sevostjanovs, E.; Goldins, N. R.; Groma, V.; Grinberga, S.; Plaas, M.; Makrecka-Kuka, M.; Dambrova, M. Low Cardiac Content of Long-Chain Acylcarnitines in TMLHE Knockout Mice Prevents Ischaemia-Reperfusion-Induced Mitochondrial and Cardiac Damage. *Free Radic. Biol. Med.* **2021**, *177*, 370–380.
- [6] Kerner, J.; Hoppel, C. Fatty Acid Import into Mitochondria. *Biochim. Biophys. Acta - Mol. Cell Biol. Lipids* **2000**, *1486* (1), 1–17.
- [7] Ramsay, R. R.; Gandour, R. D.; Van Der Leij, F. R. Molecular Enzymology of Carnitine Transfer and Transport. *Biochim. Biophys. Acta – Protein Struct. Mol. Enzymol.* **2001**, *1546*, 21–43.
- [8] Reuter, S. E.; Evans, A. M. Carnitine and Acylcarnitines: Pharmacokinetic, Pharmacological and Clinical Aspects. *Clin. Pharmacokinet.* **2012**, *51* (9), 553–572.
- [9] Rebouche, C. J. Carnitine Function and Requirements during the Life Cycle. *FASEB J.* **1992**, *6* (15), 3379–3386.
- [10] Leśniak, R. K.; Markolovic, S.; Tars, K.; Schofield, C. J. Human Carnitine Biosynthesis Proceeds via (2S,3S)-3-Hydroxy-N ϵ -Trimethyllysine. *Chem. Commun.* **2017**, *53* (2), 440–442.
- [11] Reddy, Y. V.; Al Temimi, A. H. K.; White, P. B.; Mecinović, J. Evidence That Trimethyllysine Hydroxylase Catalyzes the Formation of (2S,3S)-3-Hydroxy-N ϵ -Trimethyllysine. *Org. Lett.* **2017**, *19* (2), 400–403.
- [12] Vaz, F. M.; van Vlies, N. Chapter 13. Dioxygenases of Carnitine Biosynthesis: 6- N -Trimethyllysine and γ -Butyrobetaine Hydroxylases. In *2-Oxoglutarate-Dependent Oxygenases*; **2015**; pp 324–337.
- [13] Herr, C. Q.; Hausinger, R. P. Amazing Diversity in Biochemical Roles of Fe(II)/2-Oxoglutarate Oxygenases. *Trends Biochem. Sci.* **2018**, *43* (7), 517–532.
- [14] Islam, M. S.; Leissing, T. M.; Chowdhury, R.; Hopkinson, R. J.; Schofield, C. J. 2-Oxoglutarate-Dependent Oxygenases. *Annu. Rev. Biochem.* **2018**, *87* (1), 585–620.
- [15] Tars, K.; Rumnieks, J.; Zeltins, A.; Kazaks, A.; Kotelovica, S.; Leonciks, A.; Sharipo, J.; Viksna, A.; Kuka, J.; Liepinsh, E.; Dambrova, M. Crystal Structure of Human Gamma-Butyrobetaine Hydroxylase. *Biochem. Biophys. Res. Commun.* **2010**, *398* (4), 634–639.
- [16] Leung, I. K. H.; Krojer, T. J.; Kochan, G. T.; Henry, L.; von Delft, F.; Claridge, T. D. W.; Oppermann, U.; McDonough, M. a.; Schofield, C. J. Structural and Mechanistic Studies on γ -Butyrobetaine Hydroxylase. *Chem. Biol.* **2010**, *17* (12), 1316–1324.

- [17] Rydzik, A. M.; Leung, I. K. H.; Kochan, G. T.; McDonough, M. A.; Claridge, T. D. W.; Schofield, C. J. Oxygenase-Catalyzed Desymmetrization of N , N -Dialkyl-Piperidine-4-Carboxylic Acids. *Angew. Chemie Int. Ed.* **2014**, *53* (41), 10925–10927.
- [18] Rydzik, A. M.; Chowdhury, R.; Kochan, G. T.; Williams, S. T.; McDonough, M. A.; Kawamura, A.; Schofield, C. J. Modulating Carnitine Levels by Targeting Its Biosynthesis – Selective Inhibition of γ -Butyrobetaine Hydroxylase. *Chem. Sci.* **2014**, *5* (5), 1765.
- [19] Wang, Y.; Reddy, Y. V.; Al Temimi, A. H. K.; Venselaar, H.; Nelissen, F. H. T.; Lenstra, D. C.; Mecinović, J. Investigating the Active Site of Human Trimethyllysine Hydroxylase. *Biochem. J.* **2019**, *476* (7), 1109–1119.
- [20] The PyMOL Molecular Graphics System, Version 2.5.2, **2021**.
- [21] UniProt. P05413 . FABPH_HUMAN.
<https://www.uniprot.org/uniprotkb/P05413/entry#sequences>.
- [22] Zimmerman, A. W.; Veerkamp, J. H. New Insights into the Structure and Function of Fatty Acid-Binding Proteins. *Cell. Mol. Life Sci.* **2002**, *59* (7), 1096–1116.
- [23] Binias, B.; Danneberg, H.; Mcwhir, J.; Mullins, L.; Clark, A. J. Requirement for the Heart-type Fatty Acid Binding Protein in Cardiac Fatty Acid Utilization. *FASEB J.* **1999**, *13* (8), 805–812.
- [24] Storch, J.; Thumser, A. E. A. The Fatty Acid Transport Function of Fatty Acid-Binding Proteins. *Biochim. Biophys. Acta – Mol. Cell Biol. Lipids* **2000**, *1486* (1), 28–44.
- [25] Scapin, G.; Young, A. C. M.; Kromminga, A.; Veerkamp, J. H.; Gordon, J. I.; Sacchettini, J. C. High Resolution X-Ray Studies of Mammalian Intestinal and Muscle Fatty Acid-Binding Proteins Provide an Opportunity for Defining the Chemical Nature of Fatty Acid: Protein Interactions. *Mol. Cell. Biochem.* **1993**, *123* (1–2), 3–13.
- [26] Lassen, D.; Lucke, C.; Kveder, M.; Mesgarzadeh, A.; Schmidt, J. M.; Specht, B.; Lezius, A.; Spener, F.; Ruterjans, H. Three-Dimensional Structure of Bovine Heart Fatty-Acid-Binding Protein with Bound Palmitic Acid, Determined by Multidimensional NMR Spectroscopy. *Eur. J. Biochem.* **1995**, *230* (1), 266–280.
- [27] Matsuoka, D.; Sugiyama, S.; Murata, M.; Matsuoka, S. Molecular Dynamics Simulations of Heart-Type Fatty Acid Binding Protein in Apo and Holo Forms, and Hydration Structure Analyses in the Binding Cavity. *J. Phys. Chem. B* **2015**, *119* (1), 114–127.
- [28] Kazaks, A.; Makrečka-Kuka, M.; Kuka, J.; Voronkova, T.; Akopjana, I.; Grinberga, S.; Pugovics, O.; Tars, K. Expression and Purification of Active, Stabilized Trimethyllysine Hydroxylase. *Protein Expr. Purif.* **2014**, *104* (September), 1–6.
- [29] Rydzik, A. M.; Leung, I. K. H.; Kochan, G. T.; Loik, N. D.; Henry, L.; McDonough, M. A.; Claridge, T. D. W.; Schofield, C. J. Comparison of the Substrate Selectivity and Biochemical Properties of Human and Bacterial γ -Butyrobetaine Hydroxylase. *Org. Biomol. Chem.* **2014**, *12* (33), 6354–6358.
- [30] Jumper, J.; Evans, R.; Pritzel, A.; Green, T.; Figurnov, M.; Ronneberger, O.; Tunyasuvunakool, K.; Bates, R.; Židek, A.; Potapenko, A.; Bridgland, A.; Meyer, C.; Kohl, S. A. A.; Ballard, A. J.; Cowie, A.; Romera-Paredes, B.; Nikolov, S.; Jain, R.; Adler, J.; Back, T.; Petersen, S.; Reiman, D.; Clancy, E.; Zielinski, M.; Steinegger, M.; Pacholska, M.; Berghammer, T.; Bodenstein, S.; Silver, D.; Vinyals, O.; Senior, A. W.; Kavukcuoglu, K.; Kohli, P.; Hassabis, D. Highly Accurate Protein Structure Prediction with AlphaFold. *Nature* **2021**, *596* (7873), 583–589.
- [31] Varadi, M.; Anyango, S.; Deshpande, M.; Nair, S.; Natassia, C.; Yordanova, G.; Yuan, D.; Stroe, O.; Wood, G.; Laydon, A.; Židek, A.; Green, T.; Tunyasuvunakool, K.; Petersen, S.; Jumper, J.; Clancy, E.; Green, R.; Vora, A.; Lutfi, M.; Figurnov, M.; Cowie, A.; Hobbs, N.; Kohli, P.; Kleywegt, G.; Birney, E.; Hassabis, D.; Velankar, S. AlphaFold

- Protein Structure Database: Massively Expanding the Structural Coverage of Protein-Sequence Space with High-Accuracy Models. *Nucleic Acids Res.* **2022**, *50* (D1), D439–D444.
- [32] Zelencova, D. ϵ -Trimetillizīna Hidroksilāze. Inhibitoru Meklējumi, Rīgas Tehniskā universitāte, **2015**.
- [33] Fowler, D. M.; Stephany, J. J.; Fields, S. Measuring the Activity of Protein Variants on a Large Scale Using Deep Mutational Scanning. *Nat. Protoc.* **2014**, *9* (9), 2267–2284.
- [34] Zelencova-Gopejenko, D.; Grandane, A.; Loza, E.; Lola, D.; Sipola, A.; Liepinsh, E.; Arsenyan, P.; Jaudzems, K. Binding versus Enzymatic Processing of ϵ -Trimethyllysine Dioxygenase Substrate Analogues. *ACS Med. Chem. Lett.* **2022**, *13* (11), 1723–1729.
- [35] Tars, K.; Leitans, J.; Kazaks, A.; Zelencova, D.; Liepinsh, E.; Kuka, J.; Makrecka, M.; Lola, D.; Andrianovs, V.; Gustina, D.; Grinberga, S.; Liepinsh, E.; Kalvinsh, I.; Dambrova, M.; Loza, E.; Pugovics, O. Targeting Carnitine Biosynthesis: Discovery of New Inhibitors against γ -Butyrobetaine Hydroxylase. *J. Med. Chem.* **2014**, *57* (6), 2213–2236.
- [36] Al Temimi, A. H. K.; Pieters, B. J. G. E.; Reddy, Y. V.; White, P. B.; Mecinović, J. Substrate Scope for Trimethyllysine Hydroxylase Catalysis. *Chem. Commun.* **2016**, *52* (87), 12849–12852.
- [37] Rydzik, A. M.; Leung, I. K. H.; Kochan, G. T.; Thalhammer, A.; Oppermann, U.; Claridge, T. D. W.; Schofield, C. J. Development and Application of a Fluoride-Detection-Based Fluorescence Assay for γ -Butyrobetaine Hydroxylase. *ChemBioChem* **2012**, *13* (11), 1559–1563.
- [38] Zelencova-Gopejenko, D.; Videja, M.; Grandane, A.; Pudnika-Okinčica, L.; Sipola, A.; Vilks, K.; Dambrova, M.; Jaudzems, K.; Liepinsh, E. Heart-Type Fatty Acid Binding Protein Binds Long-Chain Acylcarnitines and Protects Against Lipotoxicity. *Int. J. Mol. Sci.* **2023**, *24* (6), 5528.
- [39] Matsuoka, S.; Sugiyama, S.; Matsuoka, D.; Hirose, M.; Lethu, S.; Ano, H.; Hara, T.; Ichihara, O.; Kimura, S. R.; Murakami, S.; Ishida, H.; Mizohata, E.; Inoue, T.; Murata, M. Water-Mediated Recognition of Simple Alkyl Chains by Heart-Type Fatty-Acid-Binding Protein. *Angew. Chemie Int. Ed.* **2015**, *54* (5), 1508–1511.
- [40] Spector, A. A.; John, K.; Fletcher, J. E. Binding of Long-Chain Fatty Acids to Bovine Serum Albumin. *J. Lipid Res.* **1969**, *10*, 56–67.
- [41] Malik, W. U.; Jain, A. K. Electrometric Determination of Critical Micelle Concentration of Soap Solutions. *J. Electroanal. Chem. Interfacial Electrochem.* **1967**, *14* (1), 37–41.
- [42] Hoerr, C. W.; Pool, W. O.; Ralston, A. W. The Effect of Water on the Solidification Points of Fatty Acids. Solubility of Water in Fatty Acids. *Oil Soap* **1942**, *19* (7), 126–128.
- [43] Sharp, K. Entropy--Enthalpy Compensation: Fact or Artifact? *Protein Sci.* **2001**, *10* (3), 661–667.
- [44] Ford, D. M. Enthalpy-Entropy Compensation Is Not a General Feature of Weak Association. *J. Am. Chem. Soc.* **2005**, *127* (46), 16167–16170.
- [45] Goldberg, R. N.; Kishore, N.; Lennen, R. M. Thermodynamic Quantities for the Ionization Reaction of Buffers. *J. Phys. Chem. Ref. Data* **2002**, *31* (2), 231–370.
- [46] Ho, J. K.; Duclos, R. I.; Hamilton, J. A. Interactions of Acyl Carnitines with Model Membranes. *J. Lipid Res.* **2002**, *43* (9), 1429–1439.
- [47] Yalkowsky, S. H.; Zografī, G. Some Micellar Properties of Long-Chain Acylcarnitines. *J. Colloid Interface Sci.* **1970**, *34* (4), 525–533.
- [48] Williamson, M. P. Using Chemical Shift Perturbation to Characterise Ligand Binding. *Prog. Nucl. Magn. Reson. Spectrosc.* **2013**, *73*, 1–16.
- [49] Hobbs, B.; Drant, J.; Williamson, M. P. The Measurement of Binding Affinities by NMR

- Chemical Shift Perturbation. *J. Biomol. NMR* **2022**, *76* (4), 153–163.
- [50] Schrödinger Release 2022-1: Induced Fit Docking Protocol; Glide, Schrödinger, LLC, New York, NY, 2021; Prime, Schrödinger, **2021**.
- [51] Sherman, W.; Day, T.; Jacobson, M. P.; Friesner, R. A.; Farid, R. Novel Procedure for Modeling Ligand/Receptor Induced Fit Effects. *J. Med. Chem.* **2006**, *49* (2), 534–553.

ACKNOWLEDGEMENTS

The development of this work would not have been possible without the participation of many other people. I would like to thank these people for their selfless work, cooperation, and knowledge sharing!

First of all, I would like to express my deepest gratitude to my first scientific supervisor, Dr. habil. chem. Edvards Liepiņš, who introduced me to the scientific world, inspired and supported me in the beginning during my bachelor's and master's degree studies, as well as in the beginning of my doctoral studies. It is very sorrowful that prof. Edvards Liepiņš has passed away, however, he will never be forgotten and the memory of him will stay in author's heart forever.

Secondly, I would like to thank the scientific supervisor of the work, prof. Dr. chem. Kristaps Jaudzems, for valuable ideas and discussions during the development of the work!

Special thanks to my colleagues at the Latvian Institute of Organic Synthesis Dr. chem. Pavel Arsenyan, prof. Dr. pharm. Maija Dambrova, and Dr. pharm. Edgars Liepiņš for valuable discussions, recommendations, and contributions to the development of joint publications.

I would like to express my gratitude to the people who helped in achieving the results of the work: Dr. chem. Aiga Grandana and Dr. chem. Einars Ložs for the synthesis of the compounds, Melita Vidēja and to Ph. D. Kārlis Vilks for biological activity and cell tests.

I sincerely thank the staff of the Latvian Biomedical research and study centre, Dr. biol. Andris Kazāks and prof. Dr. biol. Kaspars Tārs, for obtaining genetic and biological materials, for the help in the work with BBOX mutants, and valuable advice and discussions that educated me in the field of molecular biology.

I would like to thank prof. Ph. D. Amedeo Caflisch and Ph. D. Carmen Esposito, who introduced me to the latest computing methods during my visit to the University of Zurich as part of the "InnovaBalt" project.

Special thanks to my colleagues from the NMR group of the Department of Physical Organic Chemistry for valuable suggestions and many stimulating discussions.

I would also like to thank Riga Technical University, which is my *Alma Mater*!

Heartfelt thanks to the family and special thanks to Aleksejs for his endless patience and support throughout my doctoral studies.

Finally, I would like to thank the State Research Program "Biomedicine for Public Health" project No. 2 "Molecular mechanisms of diabetes and cardiovascular complications, pharmacogenetics and new therapeutic agents", for the science and technology development project of the European Union 7th framework program "InnovaBalt" and the Latvian Institute of Organic Synthesis (internal student grants no. IG-2020-02, IG-2021-02, IG-2022-04, and IG-2023-04) for the financial support during doctoral studies.



Diāna Zeļencova-Gopejenko was born in Riga in 1990. She obtained Bachelor and Master of Science in Engineering degrees in Chemical Technology from Riga Technical University in 2013 and 2015, respectively. She has been working in Latvian Institute of Organic Synthesis since 2011. She is currently a scientific assistant in the Laboratory of Structural Biology and Drug Design (former Laboratory of Physical Organic Chemistry) led by Dr. chem. Kristaps Jaudzems. During doctoral studies she studied computational chemistry in the University of Zurich (InnovaBalt project) and structural biology in the University of Tromsø (within the framework of ERASMUS+). Her main research interests include protein structural studies and new drug design by means of nuclear magnetic resonance, crystallography, and computational methods. She has co-authored nine original publications indexed in *Scopus* and *Web of Science*.